Chapter 16

Dynamics of Molecular Motors

"Like a flash of lightning and in an instant the truth was revealed. I drew with a stick on the sand the diagrams of my motor." - Nikola Tesla

Chapter Overview: In Which the Dynamics of Molecular Motors Are Studied Using Rate Equations

The question of cellular dynamics has arisen throughout the book in a number of different contexts. One of the conclusions we have drawn in our analysis is that active transport plays an important role in mediating cellular life. Molecular motors are key tools used by the cell to perform active transport and to maintain its nonequilibrium character. In particular, we interest ourselves in molecular machines that can perform work, usually by the consumption of ATP. This chemomechanical coupling will be the centerpiece of the present chapter. We begin by considering several different classes of molecular motors and the cellular processes they mediate. A vast array of different classes of experiments ranging from structure determination to single-molecule biophysics have resulted in a range of quantitative data on motors that we examine systematically. We then use rate equations to characterize the dynamics of motors.

16.1 The Dynamics of Molecular Motors: Life in the Noisy Lane

Directed and purposeful movement is one of the properties we most closely associate with living organisms. Even organisms that appear immotile to the naked eye such as green plants are very busy on the cellular level, exhibiting rapid directed movements of organelles such as chloroplasts and segregation of chro-

mosomes during cell division. The past several chapters have largely focused on diffusion and random walks as modes of motion, but these are clearly insufficient to explain directed movements such as chromosome segregation or muscle contraction. Nonrandom movements cost energy! They demand mechanisms that convert chemical energy into mechanical energy (work). In chap. 5, we have described the forms of chemical energy storage in cells including high-energy covalent bonds such as the phosphoanhydride bonds in ATP and ion gradients across membranes (or more generally, concentration gradients). The focus of this chapter will be on molecular motors that are able to use one of these forms of chemical energy to generate a mechanical force acting over a defined distance in a defined direction. In our exploration of these molecular motors, we will blend many of the physical and biological principles encountered in previous chapters ranging from beam theory through rate equations.

One fascinating feature of the motors found in cells is their structural and functional diversity. Nevertheless, many different kinds of motors share similar fundamental physical mechanisms, so analysis of one motor can frequently shed light on the functioning of other motors that are evolutionarily unrelated and are used for distinct biological purposes. For convenience, we will separate our analysis of motors into four broad classes:

i) Translational motors. These are motors that move in a one-dimensional fashion, by stepping along a linear "track" as a substrate. Motors in this class include myosin, which causes muscle contraction by walking along actin filaments, and helicases, which move along DNA and use energy to unwind the double helix.

ii) Rotary motors. These remarkable motors are usually embedded in the cell membrane and generate torque by rotation of mechanical elements. The best-understood rotary motor in biology is the bacterial flagellar motor, shown in fig. 3.18 (pg. 153).

iii) Polymerization motors. As we began to explore in the preceding chapter, energy can be released during the process of subunit polymerization and depolymerization. Both actin assembly and microtubule assembly are harnessed by cells to generate force directly, as well as to provide linear tracks for other force-generating translational motors.

iv) Translocation motors. These motors involve threading a structure such as DNA or an unfolded protein through a hole and then pushing it or pulling it through the hole, frequently (though not always) across a membrane. The importing of proteins into specific cellular organelles, such as the mitochondrion, frequently requires the action of translocation motors.

This scheme for dividing motors into four classes will simplify our modeling efforts later in the chapter, but this list is neither comprehensive nor mutually exclusive. Some important motors combine features of more than one class. For example, RNA polymerase moves along its DNA substrate like a translational motor, but uses energy derived from polymerization of nucleotide subunits. The motor that packages bacteriophage DNA into the capsid is thought to combine features of both rotary and translocation motors. Also, there are several kinds of force-generating systems known to operate in specialized cells that do not fit

easily within this framework. A famous example is the sperm of the horseshoe crab, which carries a coiled prestressed spring that can uncoil rapidly when triggered to pierce the jelly coat of the horseshoe crab egg during fertilization. We will not attempt to explore the mechanisms of such exotic motors here, although they must obey the same physical principles as the more familiar motors that we will use as our examples.

Our plan in this chapter is to examine the structure and function of these different classes of motor and then to show how simple rate equations can be used to understand many aspects of their operation. The study of biological motors has been a fertile area for the fusion of biology and physics in research, because understanding their function demands an integration of biochemistry with mechanics. Characterization of the properties of a molecular motor such as kinesin, a translational motor that moves along microtubules, requires measuring the biochemical rate constants associated with its hydrolysis of ATP, but also physical properties such as the speed with which it moves and the amount of force that it can generate. Because of the small size of most biological motor proteins (typically a few nanometers) and the fact that they operate under conditions where thermal motions are significant, measurements of physical motor properties such as speed and force has been technically challenging. As we will see, numerous clever and elegant measurement techniques that exploit a wide range of physics concepts have been developed for this purpose, largely by teams of biologists and physicists working together.

Within a unified physical framework where molecular motors are treated as tiny machines that convert chemical energy into mechanical work, the characteristics of different motors can be compared and the mechanisms of their inner gearboxes deduced. As an example, fig. 16.1 shows the behavior of three different motors, kinesin, RNA polymerase, and the phage packaging motor, when they are subjected to increasing loads. Just like human-manufactured motors, molecular motors tend to slow down when they are forced to do more work, but the three different motors slow down in distinct ways. The biological function of motors depends on the way that they convert the energy released from a chemical reaction to the conformational change that causes movement and generates force. Conversely, external forces applied to moving motors can affect their biochemical reaction rates. Therefore, the motor's speed depends on the applied force in a way that must reflect its mechanochemical energy conversion mechanism. As shown in the graph, RNA polymerase tends to move at top speed as its load increases until it reaches a threshold where its speed slows suddenly and stalls. In contrast, the phage packaging motor slows down very gradually with increasing force, and kinesin exhibits a complex force-velocity relationship somewhere in between. Later in the chapter, we will see how different physical models for the coupling between mechanics and biochemistry inside a molecular motor can predict different shapes for these characteristic force-velocity curves. Before proceeding to the modeling, we will begin with a brief tour of the biological roles and characteristics of the four major motor classes.

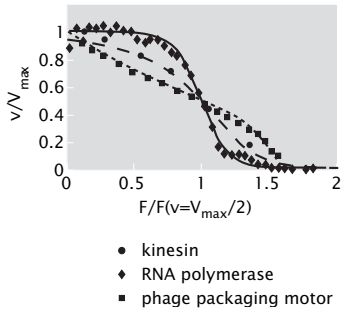

Figure 16.1: Effects of load force on motor velocity for kinesin, RNA polymerase, and the bacteriophage packaging motor. For all three motors, the speed has been normalized to the maximum speed (v/V_{max}) and the force has been normalized to the force where the speed is decreased to half its maximum ($F(v = V_{max}/2)$). The different shapes of the force-velocity curves imply distinct mechanisms. (Adapted from C. Bustamante *et al.*, Ann. Rev. Biochem., 73:705, 2004.)

16.1.1 Translational Motors: Beating the Diffusive Speed Limit

One of the most important and familiar classes of molecular motors are those associated with the cytoskeleton, specifically with microtubules and actin filaments. As we have already seen throughout the book, these motors are responsible for motile processes as diverse as the directed transport of vesicles in individual cells to the running, swimming and flying of animals on the basis of muscle contractions. These translational cytoskeletal motors can be classified into three protein families, myosin, kinesin, and dynein, one member of each being shown in fig. 16.2. Because both microtubules and actin filaments are constructed from asymmetric subunits that self-assemble by binding to each other in a head-to-tail orientation, the tracks have a distinct structural polarity, and each type of motor is able to move in one direction. Members of the dynein protein family, for example, move along microtubules toward the minus end, while most members of the kinesin family move in the opposite direction, toward the plus end (although there are a few special types of kinesin that are minus-end directed). Myosin family members all move along actin filaments, mostly toward the barbed end (equivalent to the microtubule plus end), but with a few exceptions that move toward the pointed end.

Each of these motors moves along its substrate track by taking a series of discrete steps of fixed size. Each mechanical step is tightly coupled to a single biochemical cycle of ATP binding, hydrolysis, and product release. The net speed of a translation motor, then, is the product of its step size and the number

of steps it can take per unit time. Another important feature of translation motors is their processivity, that is, the number of steps that a single motor can take along a single filament before it falls off. Some translation motors, such as RNA polymerase, are extremely processive, so that an entire messenger RNA molecule that may include thousands of nucleotide bases can be synthesized by one polymerase in a single run. Other motors are much less processive. As we will see below, the myosin motor involved in muscle contraction typically takes only one or two steps along its actin filament before it falls off; this low processivity is important for its normal biological function. The amount of force that can be exerted by a single motor taking a single step is ultimately limited by the amount of chemical energy liberated by hydrolysis of a single molecule of ATP.

- **Estimate: Force exerted by a single motor step.** The kinesin motor moves 8 nm per ATP hydrolysis event. As a result, we can estimate the force exerted by the motor as

$$F_{max} = \frac{\text{free energy of ATP hydrolysis}}{\text{step size}} \approx \frac{20\ k_BT}{8\ \text{nm}} \approx 10\ \text{pN},$$

  where we have used our usual rule of thumb that the thermal energy scale is $k_BT \approx 4$ pN nm. Of course, this is an overestimate because we have assumed that the entirety of the free energy offered up by ATP hydrolysis can be converted into mechanical work; real motors may work with lower efficiency.

Each of the three major cytoskeletal motor families contains numerous distinct members that are specialized for different functions in the cell, for example different kinesin family members bind to different cargoes and move along microtubules at different speeds. Overall, the three classes of motor share similar domain organization, as illustrated in fig. 16.2. One unifying structural theme is the existence of an ATP-binding domain, called the motor head domain, in the parts of the motors that are able to bind to their target filaments. This domain catalyzes the hydrolysis of ATP and undergoes a conformational change that is guided and amplified into a large scale conformational change of the whole molecule, allowing it to make a step along its linear track. In order for movement to be productive, the cycle of ATP hydrolysis must be coupled to a second cycle of binding and unbinding to the track. The three sample motors shown here all have two heads, but some motors have just one, or even three. At the opposite end of the molecule, the tail domain is able to bind to cargo. Within each protein family, the motor head domains are evolutionarily more conserved than the cargo-binding tail domains. This makes sense, because all the motors of a given class walk along the same type of track, but may carry different kinds of cargo.

A schematic of the diversity of trafficking action associated with these motors is shown in fig. 16.3. A concrete example of this kind of trafficking is seen in neurons, where microtubule-based motors carry vesicles, proteins and mRNA

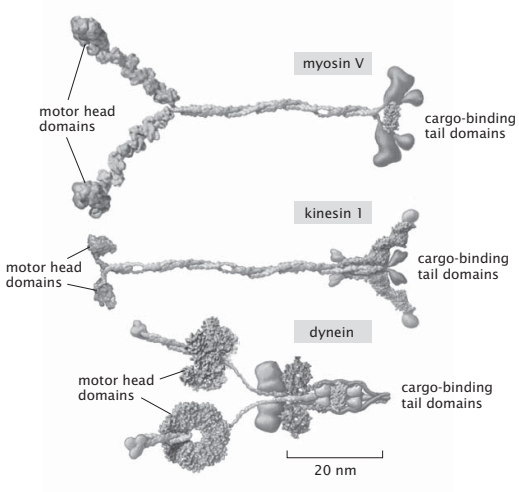

Figure 16.2: Key classes of translational motor. Top: a myosin V molecule is one of about twenty different types of myosins that move on actin filaments. Middle: kinesin 1 is also a member of a large family of related molecular motor proteins, but these move on microtubules rather than on actin. Although myosins and kinesins have different substrates, the detailed structure of their motor heads is quite similar and they are thought to be derived from a single common molecular ancestor. Bottom: cytoplasmic dynein represents a different class of microtubule-based motors that appears to be unrelated to kinesin or myosin. (Adapted from R. D. Vale, Cell, 112:467, 2003.)

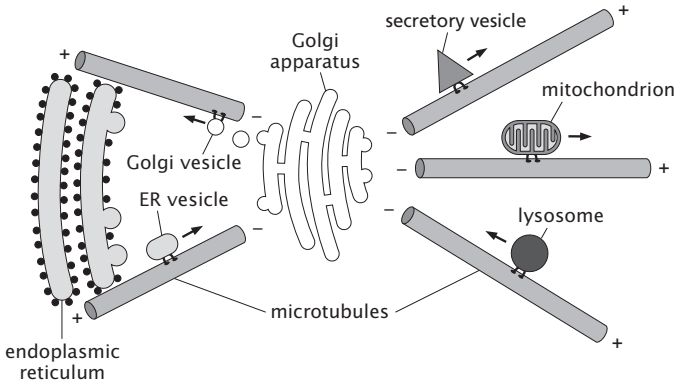

Figure 16.3: Directional transport of membrane-bound organelles. This schematic shows a few of the different types of microtubule-based organelle transport that must coexist in a typical eukaryotic cell. Different members of the kinesin and dynein motor protein families bind to distinct organelles or transport vesicles and mediate their movement through the cell. (Adapted from N. Hirokawa, Science, 279:519, 1998.)

from their sites of synthesis in the cell body to the sites of synapse formation at the far end of the axon. In a giraffe, this distance for the longest neurons in the body can be several meters, and the microtubule-based motors carry material at the rate of about 20-40 cm/day.

Yet another intriguing example of the role of translational motors in cells is in the process of cell division. Throughout the book, we have made much of the story of genome management, both in terms of the physical demands associated with having the genetic material in the right place at the right time as well as with the informational demands tied to making sure that genes are expressed when they need to be. A compelling part of that story is chromosome segregation into two daughter cells after DNA replication during the cell cycle. In this setting, translational microtubule-based motors are partially responsible for the separation of the chromosomes by the mitotic spindle during cell division, where over a dozen distinct kinesin family members collude with one another and with a cytoplasmic form of dynein to generate relative translation of the microtubules within the spindle and to position and move the chromosomes. This phenomenon was already shown in fig. 15.19 (pg. 788) and we remind the reader of it here as a shining example of the orchestrated activities of motors and their cytoskeletal partners.

The Motion of Eukaryotic Cilia and Flagella Are Driven by Translational Motors

Another example of the action of translational motors is provided by active filamentous structures in cells, which embody a subtle coupling between

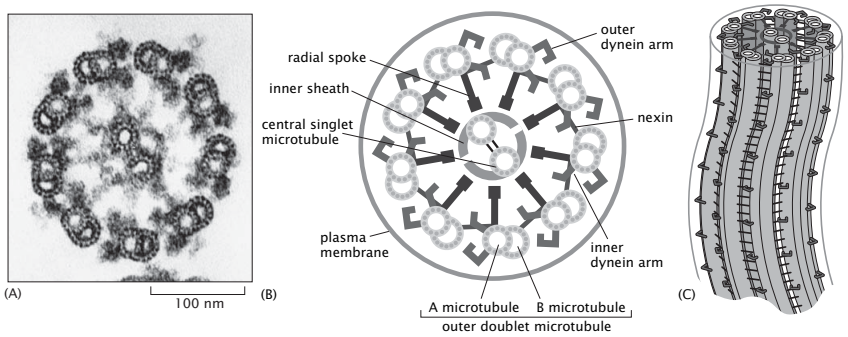

Figure 16.4: Structure of the axoneme. (A) Thin-section electron micrograph of a cross-section of the flagellum of the microscopic algae *Chlamydomonas*. (B) Diagram of the flagellar parts. The inner dynein arms and outer dynein arms are motor proteins that make the flagellum beat by sliding the microtubules relative to one another. (C) A side view of the flagellum. (A, courtesy of Lewis Tilney.)

beam-bending dynamics and translational, force-generating motors. In particular, a wide range of processes important to eukaryotic organisms are mediated by flagella and cilia, which are cell-surface projections containing bundles of microtubules crosslinked by special forms of dynein motor proteins, surrounded by the cell plasma membrane. The motion of cilia pervades the living world with examples ranging from the surfaces of embryos to the linings of various mammalian tissues to the swimming of unicellular organisms such as *Paramecium*. One familiar example is provided by the mucociliary escalator in the lungs. As a result of waves of ciliary motion, harmful materials are transported up and out of the lungs where they can be spat out or harmlessly swallowed. Paralysis of the cilia due to superviscous mucous in cystic fibrosis patients almost universally causes early death due to the inability to clear bacterial infections. Likewise, dynein paralysis due to dynein mutations in Kartagener's syndrome tends to cause early death from lung infections. The flagella in swimming cells such as sperm cells are structurally closely related to beating cilia; both are based upon beautiful structures known as axonemes. (It is important to remember that eukaryotic flagella, such as those on sperm cells, and bacterial flagella are completely different kinds of structures. The fact that they share the same name is an unfortunate historical accident.) A schematic of the microtubule and motor-based architecture of the axoneme is shown in fig. 16.4.

The way in which translational motors are harnessed to drive oscillations of structures like cilia and eukaryotic flagella is shown in fig. 16.5. The concept is that adjacent filaments in the axoneme are connected to each other both by translational motors and by linking devices that prevent much relative motion

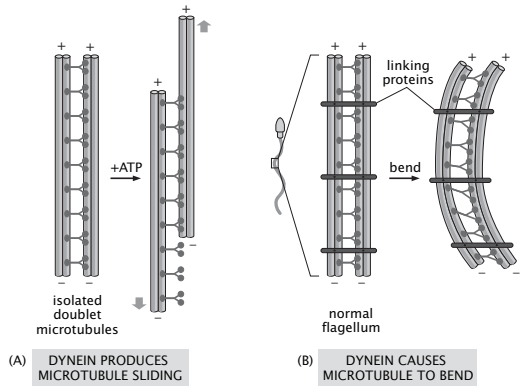

Figure 16.5: Bending of flagella and cilia due to translational motors. (A) When adjacent filaments are *not* tethered together, stepping of the motors will result in sliding of the adjacent filaments. (B) When the adjacent filaments are tethered together, stepping of the motors will result in deformation of the filaments. (Adapted from B. Alberts *et al.*, Molecular Biology of the Cell, 4th ed. New York: Garland Science, 2002.)

of these parallel filaments. As a result, when the motors make a stepping motion they produce a compressive force that induces bending. In fig. 16.5(A) we see that if two adjacent filaments are not linked, then the motion of the molecular motors will induce sliding. On the other hand, if the filaments are tied together these motors will generate bending, as is shown in fig. 16.5(B). The energetics of filament bending can be modeled using beam theory, as discussed in chap. 10. Spatial and temporal coordination of dynein motor stepping along the length of the cilium or flagellum gives rise to regular beat patterns that propagate down the structure. For example, a snapshot of the flagellum of a swimming sperm will show the flagellum bent in an elegant, near-sinusoidal curve. A moment later, the sine wave will appear to have shifted down the flagellum. The propagation of this bending wave drives the sperm head forward through its low Reynolds number environment, with an efficiency and speed that depend in part on the viscosity of the medium, as we explored in chap. 12. The ability of human sperm to swim to find an egg to fertilize, thus depends on the convergence of several important principles in physical biology.

Muscle Contraction Is Mediated by Myosin Motors

Though kinesin will usually serve as our canonical example of a translational motor, the action of translational cytoskeletal motors is probably most renowned in the context of muscles. In this case, it is the translational motor myosin which occupies centerstage as shown in fig. 16.6. The structure of muscles is an intricate combination of filaments and motors as shown in fig. 16.7. Collections of myosin molecules make thick filaments which induce relative slid-

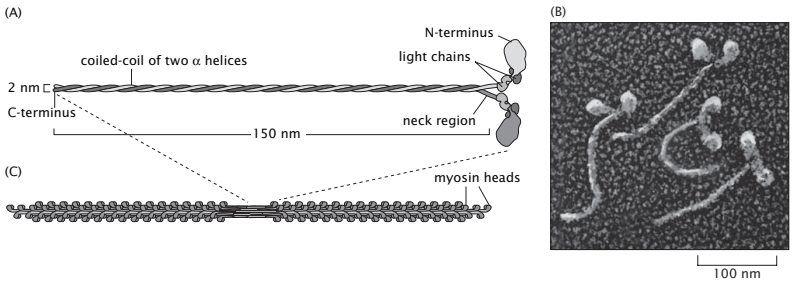

Figure 16.6: Structure of muscle myosin II. (A) Myosin II from skeletal muscle is a hexamer consisting of two extremely large heavy chains and four much smaller light chains. The heavy chains include a long coiled-coil domain at the C-terminus and the actin-binding, force-generating motor head at the N-terminus. (B) Platinum replica imaging of individual myosin molecules reveals the beautiful regularity of their structure. (C) Several hundred individual myosin II hexamers can self-assemble to form a thick filament. In this cylindrical bundle, the myosin molecules in the left half are all pointing toward the left, and those in the right half are all pointing toward the right. This antiparallel orientation is critical for muscle contraction. (A,C, adapted from B. Alberts *et al.*, Molecular Biology of the Cell, 4th ed. New York: Garland Science, 2002; B, courtesy of John Heuser.)

ing of bundles of actin. These relative motions are revealed macroscopically as muscle contractions.

- **Estimate: Myosin and Muscle Forces.** Molecular motors are molecules that consume some form of chemical energy in order to deliver mechanical work. For the translational motors of interest in the present section, the kind of information we seek in characterizing a given motor includes how fast the motor goes, how much force it can apply and how processive it is (i.e. how many steps does it take before falling off of its filament).

  A fascinating feature of muscles is that they reflect the action of many motors acting simultaneously. Given the properties of individual motors, how much force might we estimate can be applied by an array of motors such as are found in a muscle? We can develop an estimate of this force by examining the structure and function of muscles. Fig. 16.7 shows a cartoon of a muscle cell, made up of muscle fibers or myofibrils. The myofibrils are themselves composed of contractile units called sarcomeres. Myosin molecules are arranged in a cylindrically symmetric structure called the thick filament, and exert forces on the outer actin filaments. We can estimate the net force per myosin molecule by appealing to a simple picture

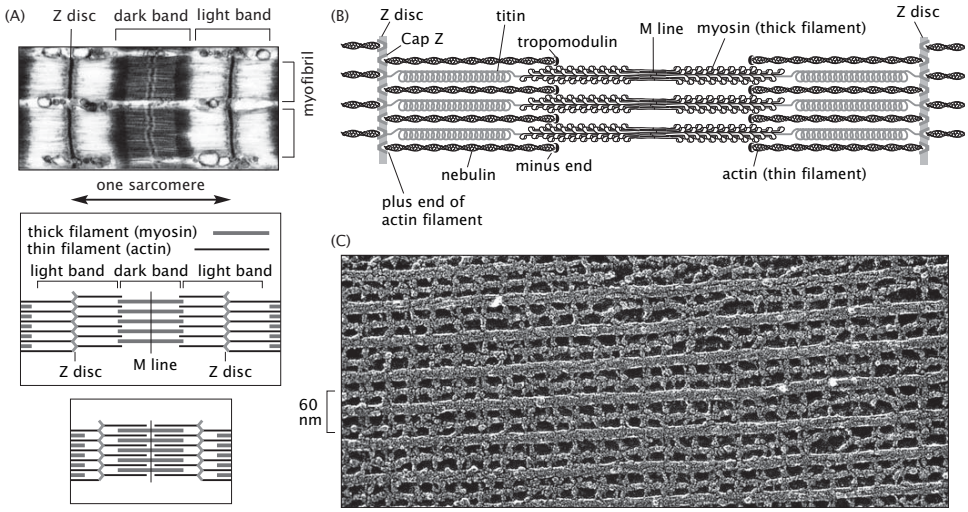

Figure 16.7: The structure of muscle. (A) Thin section electron micrograph shows the organization of a single sarcomere when a muscle is stretched. The dark band in the middle represents the location of the aligned myosin thick filaments and the light bands on the side show the position of actin. The diagrams below show the change in sarcomere length during muscle contraction. (B) The regular structure of the sarcomere depends upon proper alignment of many structural proteins. (C) A quick-freeze deep etch electron micrograph shows the extremely regular spacing of thick myosin filaments alternating with thin actin filaments and the myosin heads bridging the gap between them. (A, B, adapted from B. Alberts *et al.*, Molecular Biology of the Cell, 4th ed. New York: Garland Science, 2002; C, courtesy of John Heuser.)

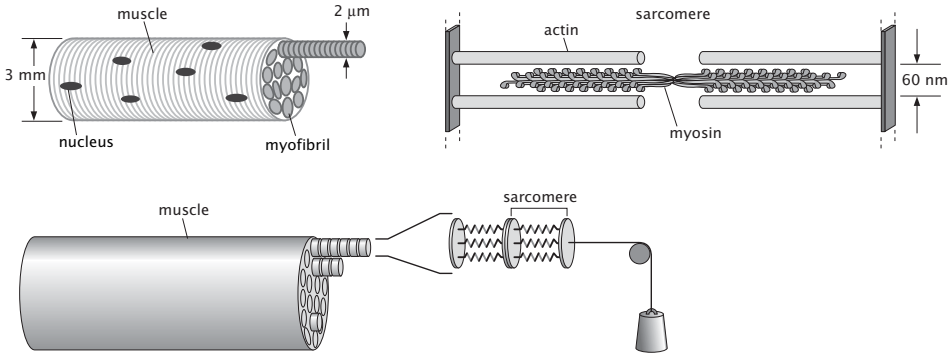

Figure 16.8: Idealization of muscle. Muscle is treated as an array of springs in series and in parallel showing how the force is shared between the different springs.

in which muscles are thought of as arrays of springs in series and parallel as shown in fig. 16.8. The number of myosins in a cross-section of muscle is roughly

$$N_{myosin} \approx \frac{\text{cross sectional area of muscle}}{\text{cross sectional area of thick filament}} \times N_{myosin/thick filament} \approx \frac{\pi(3\ cm)^2}{\pi(60\ nm)^2} \times 300 \approx 10^{14}.$$

If we assume that the force scale associated with a muscle like the biceps in the upper arm is 100 N (corresponding to lifting a 10 kg mass), and that this force is partitioned equally amongst the myosins, this results in an estimate of the force generated by a single myosin head of

$$F_{myosin} \approx \frac{10\ kg \cdot 10\ \text{m s}^{-2}}{10^{14}} = 1\ \text{pN}.$$

Despite the inexactness of several of the assumptions in this estimate, the final number of 1 pN per myosin head is of the same order of magnitude as the actual force revealed by measurements that have been made on single myosin motor proteins *in vitro*.

Translational motors of the kind introduced here serve in a huge variety of different capacities and reflect the divergence and specialization that is the hallmark of evolution. Much of what we know about these motors is the result of a variety of beautiful experiments, some of which we recount now.

- **Experiments Behind the Facts.** Our understanding of the structure, function and relatedness of different motors comes from decades of effort using a host of different techniques. Although both measurements in living cells and measurements on isolated proteins *in vitro* have contributed

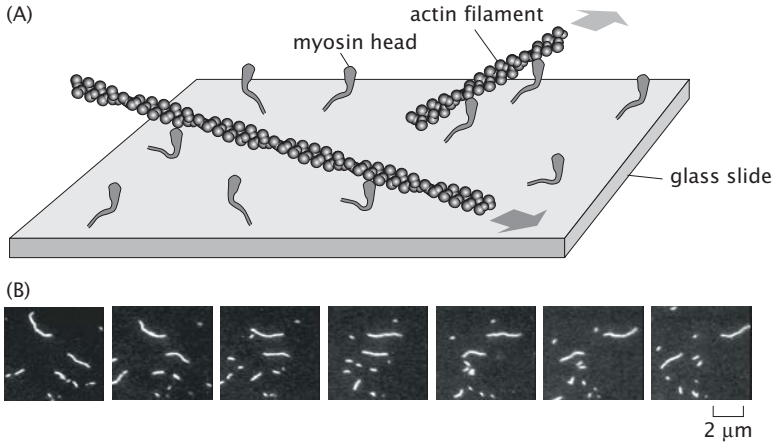

Figure 16.9: Gliding motility assay with myosin. (A) Individual motors are attached to the surface of a microscope slide and fluorescently labeled actin filaments are observed as they glide across the surface after the addition of ATP. (B) Frames from a video sequence spaced at 30 second intervals show the progress of individual filaments in many different directions. (B, courtesy of James A. Spudich.)

significantly to our understanding of motor protein action, here we will explore only *in vitro* experiments.

One of the most dramatic assays is the so-called gliding motility assay in which motors such as myosin are fixed to a microscope slide and fluorescently labeled actin filaments are then added to the system. As shown in fig. 16.9, these filaments bind to the motors and, after the addition of ATP, are then translated relative to the stationary motors. In this kind of gliding filament assay, a large number of different motor heads may bind simultaneously to the same filament and work cooperatively. This is a good imitation of *in vivo* situations such as that found for myosin II in the muscle sarcomere.

Another option for watching the movement of purified molecular motor proteins is to attach them to a bead that can be imaged with a conventional light microscope. As a result, the bead serves as a passive reporter for the actual motion of the motor itself. This geometry more closely imitates the *in vivo* situation where kinesin, for example, performs vesicle transport. Movements of the large (micrometer-scale) bead can be tracked with nanometer-scale precision, reflecting the behavior of the motor proteins. Fig. 16.10 shows an example of this kind of measurement, where the beads and the microtubules can be directly observed using DIC microscopy. Attaching a bead to a motor also offers another advantage. The bead can be trapped using optical tweezers, as illustrated in fig. 4.12

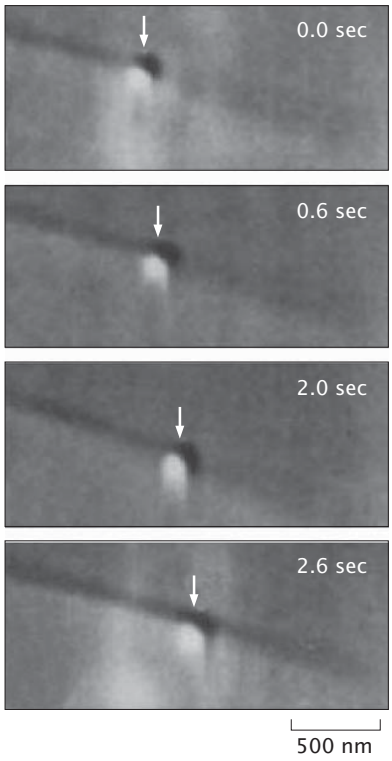

Figure 16.10: Kinesin-driven movement. A glass bead coated with kinesin motors was brought in contact with a microtubule using an optical trap. Both the microtubule and the bead can be seen using DIC microscopy and the optical trap is visible as a slightly shiny spot slightly around the bead. When the trap is shut off, the bead begins to move down the microtubule processively over several seconds. (Adapted from S. M. Block *et al.*, Nature, 348:348, 1990.)

(pg. 198), and used to apply force to the walking motor, in any direction chosen by the investigator. This is one of the most powerful techniques used to measure the response of motors to applied forces, generating data such as that shown in fig. 16.1.

Both the filament gliding assay and the bead-based assay require that the motor proteins be immobilized, on either the microscope cover slip or the bead respectively. An alternative approach is to observe the movement of individual molecules by labeling them with a small flourescent tag. For example, as shown in fig. 16.11, fluorescent molecules were attached to the heads of myosin V molecules. As a result of the actual walking of the motor, the fluorophore is observed to undergo distinct steps of a precise length. Note that from a quantitative perspective, one of the key outcomes

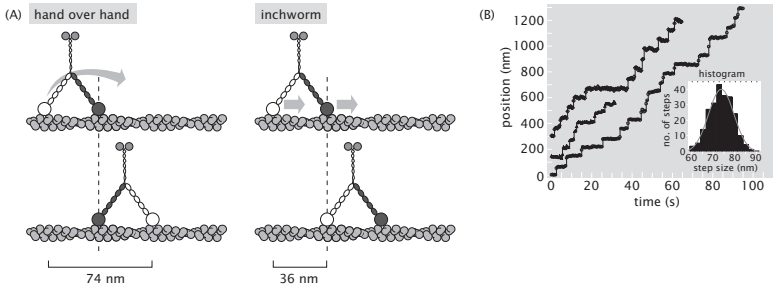

Figure 16.11: Single-molecule dynamics of myosin V stepping. (A) Cartoons showing the differences between hand-over-hand and inchworm models for motion. (B) Position as a function of time for myosin V molecules labeled with a fluorophore on one of the arms of the molecule. Three different traces from different molecules are shown. The average step size is slightly over 70 nm, consistent with a hand-over-hand stepping mechanism but inconsistent with an inchworm mechanism. (Adapted from A. Yildiz *et al.*, *Science* 300:2061, 2003.)

of single molecule experiments like these is that they provide a window on the stochastic nature of motor dynamics. For example, the time between steps of the motor is different for each step. Later in the chapter, we will calculate the expected distribution of these waiting times for simple models of motor function.

One of the applications of these particular experiments is their ability to distinguish different hypothesized mechanisms of walking such as inchworm or hand-over-hand motions. As shown in fig. 16.11 the motor has been labelled by placing a single fluorophore on one of the motor heads. In the case where the fluorophore is situated on the extremity of the motor, individual steps will be revealed as motions of the fluorophore with a step size of $\sim$ 70nm. This measurement is most consistent with a model where the two heads of myosin V take turns taking steps.

The size of the characteristic steps depends on the structure of the motor itself. An interesting demonstration of this is shown in fig. 16.12. In this experiment, the motor head domain of myosin V was progressively truncated to make it shorter and shorter. Because the conformational change of myosin that enables it to take a step involves rotation of a long, rigid "lever arm", the shortened proteins take shorter steps.

16.1.2 Rotary Motors

Not only has evolution generated an exquisite variety of translational motors, but also motors whose motions are rotational. Two of the most widely studied examples of rotary motors are the bacterial flagellar motor and ATP synthase, both of which were introduced as membrane proteins in chap. 11. Schematics

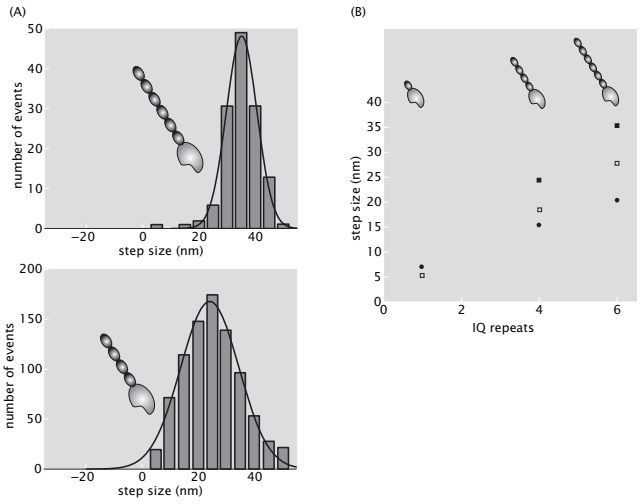

Figure 16.12: Motor step size depends on motor structure. (A) Motor heads of myosin V were purified, either in their normal state (top) or after the rotating lever arm had been shortened by protein engineering (bottom). The characteristic step size for the truncated protein is shorter than for the full-length protein. (B) For myosin V, the lever arm is built from a series of rigid subdomains called IQ repeats, so arms of different lengths can be easily constructed by including different numbers of repeats. Over a range from 1 to 6, the step size increases linearly with the number of repeats. The three different symbols show three different types of protein constructs; all follow the linear rule. (Adapted from T. J. Purcell *et al.*, Proc. Nat. Acad. Sci., 99:14159, 2002.)

of both of these motors are shown in fig. 16.13.

The bacterial flagellar motor is embedded in the cell membrane of bacterial cells and is attached to the long filamentous flagellum. A bacterial cell may have either only a single polar flagellum, like the cholera-causing pathogen *Vibrio cholerae*, or it may have several flagella distributed over the surface, like our old friend *E. coli*. When the motor rotates, it induces a rotary motion in the flagellum which propels the bacterium along in its highly viscous environs (as measured by the low Reynolds number already described in chap. 12). Interestingly, the bacterial flagellar motor uses an ion gradient (rather than ATP) as the basis of its mechanical cycle as shown in fig. 16.13. In particular, the motor is driven by a flow of hydrogen ions due to a concentration gradient between the inside of the cell and the space between the two bacterial membranes (a few exotic flagellar motors use sodium ions rather than hydrogen ions). The resulting motion has a rate in excess of 100 rotations per second. One particularly astonishing feature of this motor is that it can reverse its direction of rotation without reversing the direction of ion flow.

ATP synthase is one of the central powerhouses of living cells, found in the inner membrane of bacterial cells and also in the mitochondria of eukaryotic cells. It is an amazing molecular machine that is constructed of two different rotary motors connected to a common drive shaft. The F_0 motor of ATP synthase is similar to the flagellar rotary motor, in that it uses the energy stored in the transmembrane gradient of hydrogen ions to rotate. The F_1 motor uses ATP hydrolysis to rotate in the opposite direction. Under normal circumstances, when the transmembrane electrochemical gradient is strong, the F_0 motor generates more torque than the F_1 motor, and so the F_0 motor forces the F_1 motor to rotate in reverse, and thereby synthesize ATP from ADP plus inorganic phosphate. However, if the transmembrane electrochemical gradient is weak, the balance can tilt in the other direction, and the F_1 motor will generate more torque than F_0. Under these circumstances, the coupled motor uses ATP hydrolysis to pump hydrogen ions out of the cell.

- **Experiments Behind the Facts.** Insights into the behavior of rotary motors have been garnered from a variety of different measurements including bulk enzymatic assays, structural biology efforts and single molecule techniques. The proof of the very existence of rotary motion in living organisms was hard won, because it is technically difficult to directly observe the rotation of very small elements, or of thin filaments. One influential class of experiments involved removing the flagella from bacterial cells and then attaching the cells to glass coverslips by the flagellar root left behind. In this configuration, rotation of the flagellar motor would cause the cell itself to spin around its point of attachment to the slide, a larger-scale movement that was more easily observed in the light microscope than flagellar rotation itself. An alternative approach is to fluorescently label the flagella so that they become visible in the light microscope. An example of this kind of experiment is shown in fig. 16.14.

  Insights into the behavior of rotary motors can also be gleaned from *in*

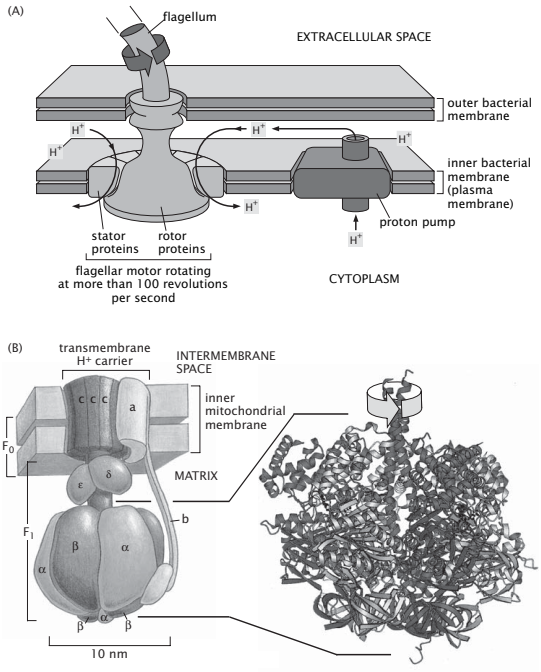

Figure 16.13: Examples of rotary motors. (A) The bacterial flagellum is like a tiny propellor driven by the gradient of hydrogen ions across the bacterial inner membrane. Continuous operation of the motor requires that the gradient be replenished by ATP-consuming proton pumps. The flagellum itself is an extremely long (10 μm) helical filament attached at its base to the motor apparatus. The motor is embedded in the bacterial inner membrane and anchored to the cell wall with a shaft passing through the outer membrane. The motor is capable of rotating in either direction at speeds up to 100 Hz. (B) ATP synthase is a rotary motor that uses the transmembrane electrical potential of the hydrogen ion gradient to drive a mechanical rotation which in turn drives the chemical synthesis of ATP from ADP and inorganic phosphate. (Adapted from B. Alberts *et al.*, Molecular Biology of the Cell, 4th ed. New York: Garland Science, 2002.)

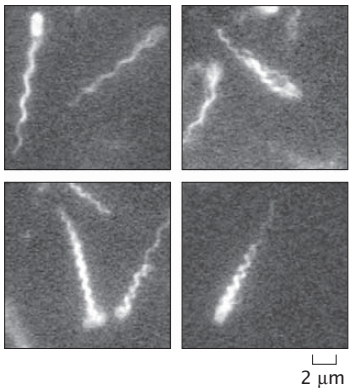

Figure 16.14: Flagellar movement in bacteria. Live bacterial cells were labeled on their surface using a fluorescent molecule revealing the helical shape of the flagella. For the different individuals shown, helical pitch and amplitude vary significantly. In a few cases, multiple helical forms can seen attached to the same bacterium resulting in frayed bundles. (Adapted from L. Turner *et al.*, J. Bacteriol., 182:2793, 2000.)

vitro measurements on single motors (as opposed to *in vivo* measurements). One of the most famed experiments of single-molecule biophysics involves the direct observation of the rotary motion of individual F_1 motors. This rotation has been measured by attaching a fluorescently labelled actin filament to the drive shaft of the motor and watching the rotation of the actin filament when the motor is provided with excess ATP (note that this is the opposite direction from its normal function in cells, where F_0 forces F_1 to run in reverse and to synthesize ATP rather than to hydrolyze it). A schematic diagram and typical data from this clever experiment are shown in fig. 16.15. These measurements revealed that the F_1 motor rotates in distinct steps of 120 degrees, tightly coupled to its ATP hydrolysis activity. The quantized nature of the steps and the tight coupling between mechanical movement and ATP hydrolysis are strongly reminiscent of the translation motors discussed in the preceding section.

16.1.3 Polymerization Motors: Pushing By Growing

The coupling of hydrolysis to force generation can take place in unexpected ways. In addition to the translational and rotary motors described above, cells have other mechanisms such as the use of polymerization of cytoskeletal filaments as a means of force generation. We will refer to these cases as polymerization motors. Several examples of polymerization motors have been shown in the previous chapter. Fig. 15.3 (pg. 756) illustrates one of our favorite examples, namely, the way in which some bacterial pathogens such as *Listeria* hijack the host

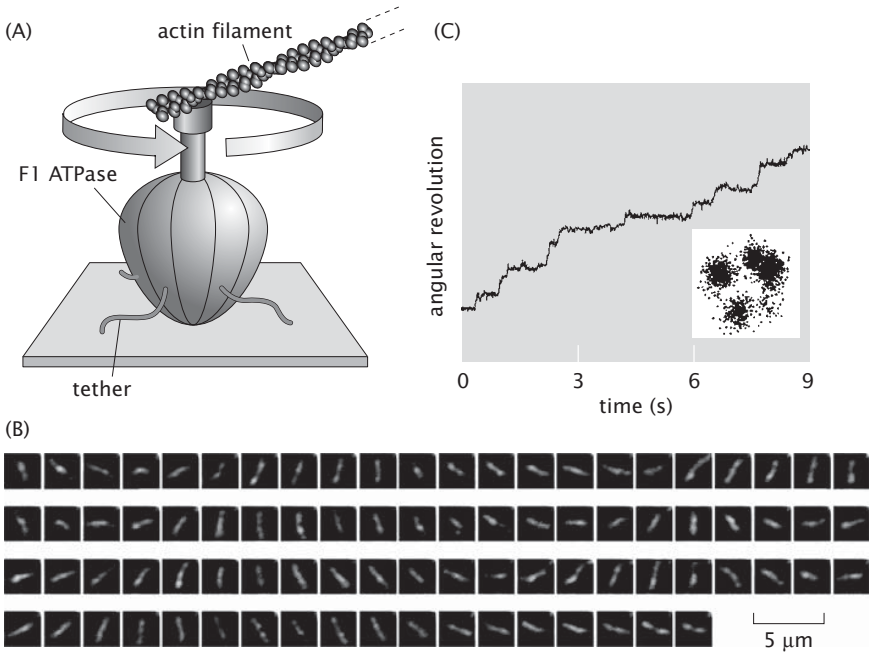

Figure 16.15: Single molecule observation of a rotary motor using actin filaments to reveal the motor rotation. (A) the F1 portion of ATP synthase is tethered to a glass slide. The top of the rotating shaft is attached to a fluorescently labeled actin filament. (B) As the F1 shaft turns, the actin filament swings around. The time interval between images is 133 msec. (C) At low ATP concentrations, it is clear that the rotation occurs in three evenly spaced angular substeps. The graph shows the angular revolution for a single actin filament over a period of a few seconds and the inset shows the positions of the filament end over a longer movie. (A, B, adapted from H. Noji *et al.*, Nature, 386:299, 1997; C, adapted from R. Yasuda *et al.*, Cell, 93:1117, 1998.)

cytoskeleton to derive their motility. Fig. 15.21 (pg. 791) is a schematic of the way that polymerization motors are thought to segregate antibiotic resistance plasmids in dividing bacteria.

In the previous chapter, we described some of the features of these cytoskeletal filaments and how rate equations can be used to describe their dynamics. However, one of the most intriguing features of these filaments that was not elaborated there is their ability to apply forces and to do mechanical work. Recall that the culmination of our discussion of the cytoskeleton was the analysis of the role of nucleotide hydrolysis in the polymerization process. For the purposes of the present chapter, this hydrolysis will be seen to contribute to the maintenance of a non-equlibrium state where soluble monomers are in excess; this unstable energetic state is necessary for polymerization motors to generate force. These examples illustrate the way in which filamentous polymerization has the consequence of mediating directed motion in cells. Note that like with translational and rotary motors, the ability of these machines to do work is ultimately tied to the fact that they consume fuel such as ATP or GTP.

16.1.4 Translocation Motors: Pushing by Pulling

Cellular life is replete with examples where macromolecules need to travel from one membrane-bound region to another. Indeed, nucleic acids, proteins, sugars and even lipids have to go from one membrane-bound region of the cell to another, or from the outside of a cell to the inside. We use the term "translocation motor" to refer to the broad class of molecular machines whose job is to mediate such transport. When viewed most broadly, this category includes the nuclear pore complex, mitochondrial import and export proteins, the proteasome, DNA packing motors in bacteriophage, ion channels, transporters, the Sec complexes and even flippases that take lipid molecules from one side of a lipid bilayer to the other and maintain highly asymmetric lipid distributions in the face of entropy.

An example of two of the speculated possible mechanisms of one of these motors is shown in fig. 16.16. The mitochondrion has served as one of the centerpiece examples throughout the book and offers us an opportunity to consider translocation motors as well. TIM and TOM are two important complexes responsible for the import and export of proteins in mitochondria. One of the mechanisms that has been proposed for membrane transport by TIM, for example, is that the unfolded peptide will be recognized in a way that permits free diffusion of the peptide into the mitochondria. As shown in fig. 16.16(A), binding partners of the translocating peptide start binding to the peptide that has already made it through the channel generating a ratchet effect. An alternative mechanism envisions a power stroke, where a molecule binds to the part of the peptide that has already diffused in and pulls it in by an ATP-driven conformational change (cross-bridge ratchet). This is depicted in fig. 16.16(B).

To drive home the significance of this kind of motor action we consider several different examples. As shown in chap. 10, bacteriophage DNA is highly pressurized in the capsid, contributing to the overall driving force behind the infection process. However, this pressure effect is apparently insufficient by

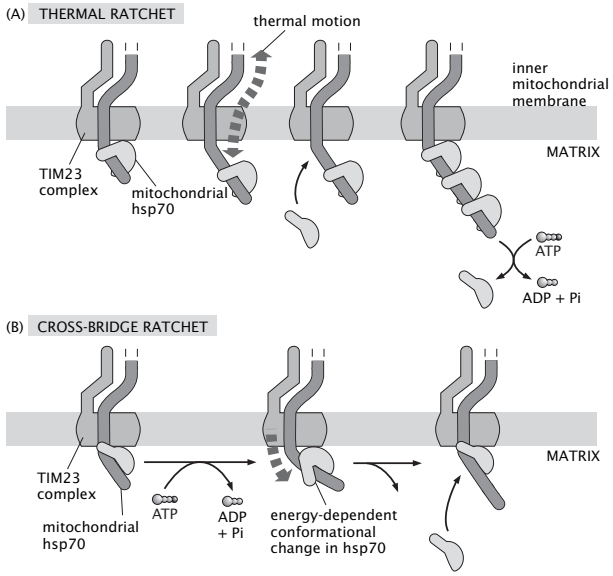

Figure 16.16: Thermal ratchet model and cross-bridge ratchet model of protein import into the mitochondria. (A) Thermal ratchet model of protein translocation. Thermal motion of the polymer in and out of the pore is biased by the presence of binding proteins on only one side of the barrier. (B) Cross-bridge ratchet model of translocation. Binding proteins on one side of the barrier may also use energy-dependent conformational changes to further ensure that the cargo polymer moves in only one direction. (Adapted from B. Alberts *et al.*, Molecular Biology of the Cell, 4th ed. New York: Garland Science, 2002.)

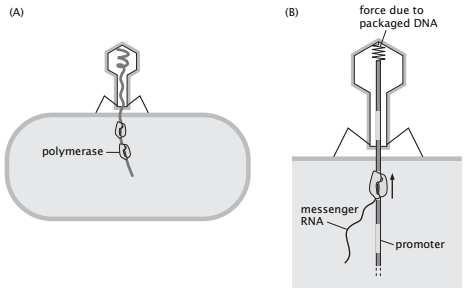

Figure 16.17: Translocation of phage DNA. (A) Illustration of the driving force on phage DNA. The packed DNA produces a driving force. In addition, the RNA polymerase can begin transcription and help to pull the DNA out. (B) Close up view of the effect of polymerase transcription on DNA translocation.

itself to mediate full translocation of the viral genome. The mechanism of translocation in the case of phage T7 is thought to be that RNA polymerase binds to a promoter located near the end that is first delivered into the bacterium and starts transcribing. The subsequent energy-dependent translocation of RNA polymerase along the DNA template contributes to pulling the bacterial genome into the host cell. This is shown schematically in fig. 16.17.

Yet another example of this same basic theme is the proteasome. The proteasome serves as the cell's protein garbage disposal, taking unwanted or misfolded polypeptides and digesting them. The protease active sites of the proteasome are sequestered on the inside of a large cylindrical complex, so that the protease activity does not accidentally degrade nonspecific targets in the cell. Delivery of polypeptide chains into the proteasome for degradation requires recognition of a specific protein tag by a cap complex that sits on both ends of the cylindrical proteasome. This cap complex uses energy derived from ATP hydrolysis to unfold the targeted polypeptide and thread it into the degrading maw of the proteasome. Once in the core of the proteasome, the polypeptides are cleaved into short peptides, and the amino acids can be recycled as building blocks for new proteins. Although protein degradation itself is not an energy-requiring process, the active unfolding of the polypeptide as it is fed into the proteasome does require the consumption of ATP.

16.2 Rectified Brownian Motion and Molecular Motors

The previous section gave a quick tour of some of the key classes of molecular motors. Now our goal is to see what kind of theoretical framework can be built

for the various observations that have been made on these motors. Though there is much that one might ask about motors, we will limit the discussion to a few key questions: What is the mean velocity of a motor and how does it depend upon the applied load? How much force can a motor exert before it will stall? How does the velocity depend upon the concentration of ATP or some other fuel? How different is the trajectory of a given motor from one experiment to the next?

One of the interesting challenges that will dictate the kinds of models we consider is shown in fig. 16.18. When viewed at very high spatial and temporal resolution, we will see that a molecular motor moves stochastically. There will be pauses between steps and sometimes the motor will lurch backwards rather than forwards. In constrast, if we look over longer time scales, the motor will appear to move steadily forward with a characteristic mean velocity. Different classes of models will capture different key features of the motor's dynamics, operating over different time and length scales.

16.2.1 The Random Walk Yet Again

Molecular Motors Can Be Thought of as Random Walkers

Throughout the book, we have seen the appeal of the broad class of random-walk models for characterizing a host of biological processes. The present section shows how driven random walk models arise naturally as a scheme for characterizing motor dynamics. We will begin by using cytoskeletal translational motors to develop these ideas, but emphasize that the conceptual treatment here is very general and can apply to rotational, polymerization, and translocation motors as well as translation motors. The basic idea is to consider the range of possible conformational states of a motor, the ways that the energy levels of the conformational states are influenced by the biochemical mechanism of energy utilization and external influences such as applied forces, and the ways that an individual motor can change from one state to another. One of the ways we will describe motor dynamics is shown in fig. 16.19. For a translational motor moving along some periodic track such as an actin filament or a microtubule, this class of models imagines n slots along the track which are each the same. Within each of these slots, the motor can be in any one of P distinct states. That is, motors are characterized by a *state space* in which the motor can occupy a set of geometric positions, and at each such position, it can occupy a set of internal structural states. This perspective is particularly transparent for a simple translational motor such as kinesin where the geometric positions correspond to different positions of the motor molecule along the microtubule, and the internal state refers to both conformational states of the motor as well as its binding to other molecules such as ATP, ADP and inorganic phosphate P_i.

The simplifying assumption that the motor position along the track can be discretized into equal-sized boxes is a reflection of the observation that real motors generally move in quantized steps of a characteristic size. We have

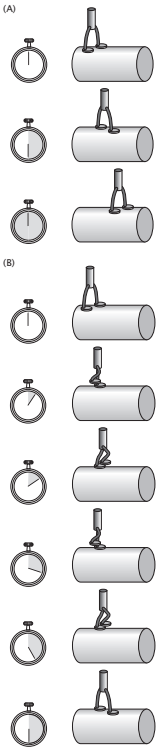

Figure 16.18: Motion of motors at different time scales. If we watch the motor with low temporal resolution, it will appear to move steadily at some mean velocity. If we watch the motor at high temporal (and spatial) resolution, we will see that its position fluctuates.

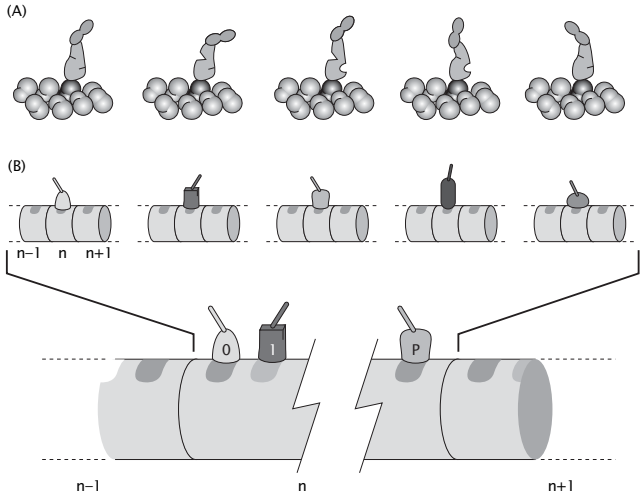

Figure 16.19: Schematic of position-state models. (A) An individual molecular motor, such as the myosin II head bound to an actin filament shown here, can exist in a wide variety of distinct conformational states. For myosin, the differences among the conformational states include the position of the lever arm, which can point either to the right or to the left, as well as the internal structure of the motor head itself, which may be different depending on whether it is bound to ATP, ADP plus inorganic phosphate, ADP alone, or no nucleotide at all, as well as on whether it is being stretched or compressed by the action of an external force or biological load. (B) A complete description of the state of an individual motor molecule must encompass its position with respect to the filament track as well as its internal conformation. The track along which the translational motor moves is divided into a set of boxes that are labelled by the parameter n. Here, each of five different protein conformations is schematized at the same position on the filament, position n. If the motor steps forward or backward, it will find itself at position n+1 or position n-1, where again it can assume any of several internal conformations. To generalize this treatment, we imagine that the motor can assume any of P distinct states at any position along the filament as shown in the bottom schematic. The description of a particular motor at any instant in time can be summarized by just two parameters, its position (n-1, n, n+1, etc.) and its internal state (0, 1, 2, etc.).

already seen this for myosin V, where each head moves about 74 nm in each cycle of ATP hydrolysis (fig. 16.11) and for F_1, which rotates in 120 degree steps (fig. 16.15).

To model the dynamics of the motor over this set of discrete states we introduce the probability $p_m(n,t)$, which is the probability that the motor is at position na along its polymer track and has internal state m at time t. The length a is defined as the distance between successive periodic positions of the track along which the translational motor moves as shown in fig. 16.19. We claim that a knowledge of the function $p_m(n,t)$ permits the calculation of quantities of interest such as the mean velocity as a function of applied load. In practice, experimenters usually perform this operation in reverse; speed is directly measured under a variety of externally imposed load forces, and the underlying kinetic rate constants are determined by fitting kinetic models to the data.

16.2.2 The One-state Model

As a first example, we adopt the simplest possible model of the motion of a motor as depicted in fig. 16.20. In this case, we assume that the motor has no internal states and simply hops from one site to the next with forward rate $k_+(F)$ and backward rate $k_-(F)$ under the action of the applied force F. $k_+(F)$ is the probability per unit time of the motor moving forward by one site, while $k_-(F)$ is the probability per unit time of the motor moving backward by one site. Note that there is an explicit dependence of these rates on the applied force, which we assume to be applied in the backward direction. We begin with this oversimplified case as a way to explore the position-state treatment, but recognize that it cannot be directly applied to any real motor, because motors must couple energy utilization (e.g. in the form of ATP hydrolysis or ion transport down an electrochemical gradient) to a mechanical conformational change, indicating that in reality they must exist in at least two states in order to do useful work. For the simplicity of the mathematical derivation, we have chosen to acknowledge the importance of energy utilization by allowing the forward rate constant $k_+(F)$ and the backward rate constant $k_-(F)$ to be different, even when the applied force F is zero. For a truly one-state motor, it would not be able to distinguish its position along the filament or distinguish a forward step from a backward step, because it would remain in the same single state regardless of its location, so there would be no way for these two rates to differ. Such a molecule would be able to move in a random walk along its filament, but could not impose a bias in either direction, and therefore could not produce useful work. So in reality, our treatment here is of a "quasi-one-state" motor, which does have different rate constants for taking a forward step vs. a backward step, but we will set aside for the moment the internal complexities of the motor that permit these differences (we will subsequently derive a two-state model that treats the differences explicitly).

At present, our goal is to determine an evolution equation for the probability distribution of the motor state $p_1(n,t) = p(n,t)$, where we have dropped

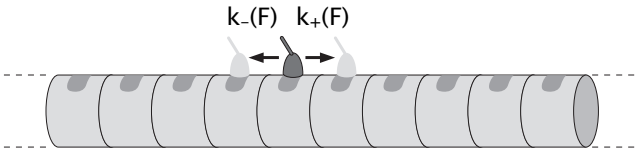

Figure 16.20: Schematic of a one state motor. The motor can only be in one state in each box. The rate constants characterize the probability that the motor will jump left or right per unit time.

reference to the label m since at each site the motor can only be in one internal state. In other words, $p(n,t)$ is the probability of finding a motor at position n at time t, where for convenience we take the time to be discretized in steps Δt.

The Dynamics of a Molecular Motor Can Be Written Using a Master Equation

At this point, we argue that the probability $p(n, t+\Delta t)$ can be gotten by summing over all of the processes that take place during time Δt, which start at time t and have as their outcome the motor ending up at site n at time $t+\Delta t$. That is, we sum over all of the individual microtrajectories available to the system with the constraint that the final state is the prescribed one. For example, the site at $n+1$ could be occupied at time t and the motor could hop backwards resulting in it being at site n in time $t+\Delta t$. As we have done throughout the book, one convenient scheme for examining dynamical processes of this sort is through "Trajectories and Weights" diagrams such as that shown in fig. 16.21.

To determine the evolution equation, we sum over all microtrajectories and the result can be written as

$$p(n,t+\Delta t) = \underbrace{k_+ \Delta t p(n-1,t)}_{\text{jump from site to left}} + \underbrace{k_- \Delta t p(n+1,t)}_{\text{jump from site to right}} + \underbrace{(1-k_-\Delta t - k_+ \Delta t)p(n,t)}_{\text{stay put}}. \tag{16.1}$$

This "master equation" adds up the probabilities of all the trajectories that lead to a given site being occupied as a result of the microscopic steps of the motor. Further, this equation can be recast in a more useful form by bringing $p(n,t)$ to the lefthand side and dividing through by Δt. This results in

$$\frac{p(n,t+\Delta t)-p(n,t)}{\Delta t} = k_+(p(n-1,t)-p(n,t))+k_-(p(n+1,t)-p(n,t)). \tag{16.2}$$

The next key point in the analysis is to think of the probability distribution as a continuous function of the position x along the filament, where the probability $p(x,t)$ for finding the motor at position x is equal to $p(n,t)$, when $x = na$. For the probability $p(x,t)$ we can use a Taylor expansion (see "The

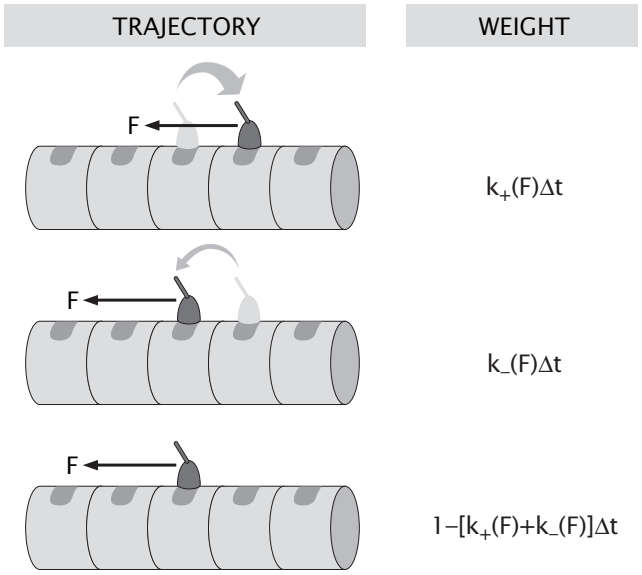

Figure 16.21: Trajectories and weights for molecular motors. The diagram shows all of the trajectories for a given motor during a time step Δt. The motor can jump forward (to the right, against the applied force) or backward (to the left, in the same direction as the applied force), or it can stay put.

Math Behind the Models" on pg. 273)

$$p(x \pm a, t) \approx p(x,t) \pm \frac{\partial p}{\partial x} a + \frac{1}{2}\frac{\partial^2 p}{\partial x^2} a^2, \tag{16.3}$$

where we ignore higher order terms. Substituting this result back into eqn. 16.2 leads to the differential equation

$$\frac{\partial p}{\partial t} = -(k_+ - k_-)\frac{\partial p}{\partial x} a + \frac{1}{2}(k_+ + k_-)\frac{\partial^2 p}{\partial x^2} a^2, \tag{16.4}$$

where we have also used the approximation

$$\frac{p(x, t+\Delta t) - p(x,t)}{\Delta t} \approx \frac{\partial p(x,t)}{\partial t}. \tag{16.5}$$

Note that this equation is of precisely the form already described in chap. 13, namely,

$$\frac{\partial p}{\partial t} = -V\frac{\partial p}{\partial x} + D\frac{\partial^2 p}{\partial x^2}, \tag{16.6}$$

where we have made the following definitions

$$V = a[k_+(F) - k_-(F)] \tag{16.7}$$

and

$$D = \frac{a^2}{2}[k_+(F) + k_-(F]. \tag{16.8}$$

What we have recovered (not surprisingly) is the equation for diffusion in the presence of a force. What we have learned is that the probability distribution $p(x,t)$ describing a one-state motor can be characterized by equation 16.6, which is a driven or biased diffusion equation also known as the Smoluchowski equation. The physical essence of this equation is that the motors move with an average velocity V. However, if we start a collection of motors on parallel filaments all at the same time (like a collection of sprinters in a race), we will find that over time, they spread out in a way characterized by the diffusion constant D. To see this explicitly, we can solve the equation.

The Driven Diffusion Equation Can Be Transformed into an Ordinary Diffusion Equation

One way to solve the equation is to perform a change of variables that turns it into the conventional diffusion equation, without a driven term, for which we already know the solution as was shown in chap. 13 (see eqn. 13.32 on pg. 689). The relevant change of variables is given by

$$\bar{t} = t \tag{16.9}$$

and

$$\bar{x} = x - Vt. \tag{16.10}$$

The fun of a transformation like this is that it amounts to shifting to a frame of reference which is moving along at the mean velocity. The derivatives appearing in the driven diffusion equation are now determined as follows. First, the time derivative is given by

$$\frac{\partial p}{\partial t} = \frac{\partial p}{\partial \bar{t}}\frac{\partial \bar{t}}{\partial t} + \frac{\partial p}{\partial \bar{x}}\frac{\partial \bar{x}}{\partial t} = \frac{\partial p}{\partial \bar{t}} - V\frac{\partial p}{\partial \bar{x}}. \tag{16.11}$$

We can perform a similar exercise with the spatial derivatives resulting in

$$\frac{\partial p}{\partial x} = \frac{\partial p}{\partial \bar{x}} \tag{16.12}$$

and

$$\frac{\partial^2 p}{\partial x^2} = \frac{\partial^2 p}{\partial \bar{x}^2}. \tag{16.13}$$

Using these transformations, we see that eqn. 16.6 takes the form

$$\frac{\partial p}{\partial \bar{t}} = D\frac{\partial^2 p}{\partial \bar{x}^2}, \tag{16.14}$$

precisely the familiar diffusion equation already discussed in detail in chap. 13.

The solution in the case of initial conditions where the motor is localized at $\bar{x} = 0$ at $t = 0$ is given by

$$p(\bar{x}, \bar{t}) = \frac{1}{\sqrt{4\pi D\bar{t}}} e^{-\frac{\bar{x}^2}{4D\bar{t}}}. \tag{16.15}$$

This can be recast in terms of the original variables as

$$p(x, t) = \frac{1}{\sqrt{4\pi Dt}} e^{-\frac{(x-Vt)^2}{4Dt}}. \tag{16.16}$$

The evolution of this probability distribution is presented in figure 16.22, where it is seen that the probability distribution broadens due to diffusion as it propagates along with a mean velocity V.

Our discussion thus far has centered on the overall dynamics of the one-state motor without reference to the actual values adopted by parameters such as $k_+(F)$ and $k_-(F)$. As was noted above, one of the primary physical aspects of the model is the presence of the asymmetric jump rates, k_+ and k_-. In particular, these jump rates are related to the force acting on the motor, shown schematically in fig. 16.23. In equilibrium we know that the ratio of the rates has to satisfy a special relation which is dictated by the characteristics of the energy landscape such as is shown in fig. 16.24. By equilibrium we mean that there is no net flux from one state, where the motor can be found with probability p_i, to the other, where the occupancy of the motor has probability p_j. For neighboring sites n and $n+1$ this condition can be written as

$$k_+ p_n = k_- p_{n+1}. \tag{16.17}$$

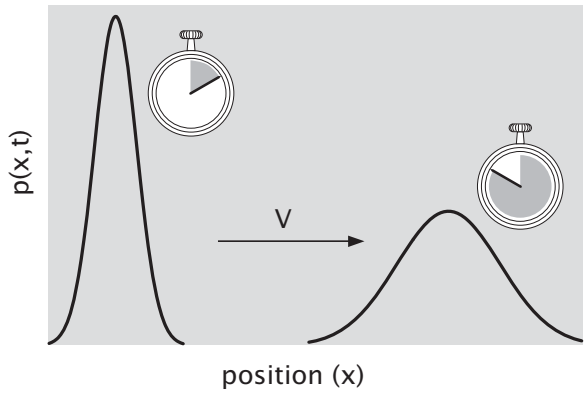

Figure 16.22: Solution to the driven diffusion equation. As time passes, the center of mass of the probability distribution moves to the right with mean velocity V. As time passes, the distribution gets wider.

Equilibrium probabilities are given by the Boltzmann formula $p_n = \exp(-\beta G_n)/Z$, where G_n is the free energy of the motor when on the nth site along the filament. Using this definition in the equilibrium condition above leads to the relation between the forward and backward rate

$$\frac{k_+}{k_-} = e^{-\beta \Delta G} \tag{16.18}$$

where the free energy change is given by $\Delta G = G_{n+1} - G_n$.

In the presence of force applied in the backward direction, the free energy of the n^{th} site is raised above the no-force value by the work of the motor against the applied force Fna, that is $G_n \rightarrow G_n + Fna$. This is depicted in fig. 16.23 in our usual way by using a pulley and mass to represent the applied force on the motor. Now applying the same reasoning as above for the no-force case, we arrive at

$$\frac{k_+(F)}{k_-(F)} = e^{-\beta(\Delta G + Fa)}. \tag{16.19}$$

The significance of this expression is described in figure 16.24 where it is seen that the effect of the force is to tilt the energy landscape and thereby change the barrier height and the allied rates.

This idea can be tested experimentally by using an optical trap to apply force to a single motor and pulling the load either forward or backward relative to the motor's preferred direction. Data from one such experiment is shown in fig. 16.25. In this case, pulling forward on myosin V increases its stepping speed by nearly ten-fold compared to pulling backward with the same force.

To say anything more about how this class of model behaves with force, we have to actually make a precise statement about how the forward and backward rates depend individually on the force. To that end, we examine several different

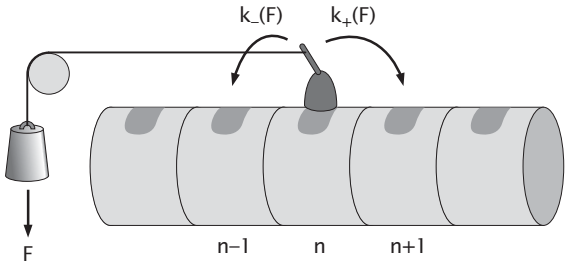

Figure 16.23: The effect of force on jump rate. A molecular motor subjected to an applied load will have its bare forward and backward jump rates modified.

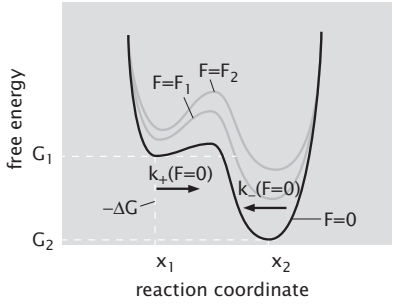

Figure 16.24: Energy landscape of a one-state model in the absence of any force (black) and when the application of forces pulling backward on the motor tilts the landscape (gray).

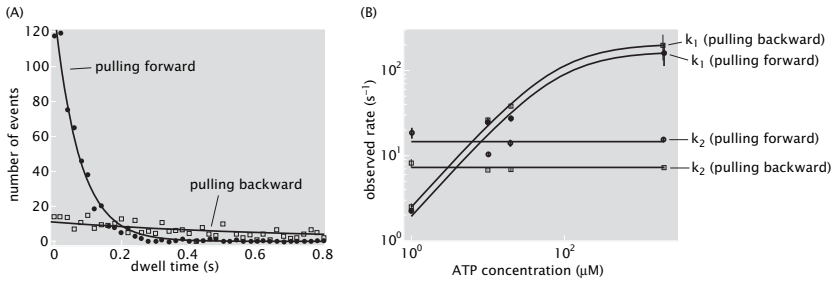

Figure 16.25: Effects of forward and backward forces on stepping rates for myosin V. (A) The average time between steps is a reflection of the motor rate. When a forward pulling force is applied to myosin V, individual steps take place in rapid succession, so the histogram of "dwell times" is dominated by very brief pauses between steps (black boxes). In contrast, the histogram of dwell times for the same motor subjected to a backward-pulling force shows very few brief pauses and many more long ones. (B) Over a range of ATP concentrations, the dwell time histograms for myosin V are best fit by a model that invokes two different internal states and two rate constants (see section 16.2.4). The rate constant for one of the state transitions, k_1, is dependent on ATP concentration but does not change with applied force (the two lines lie on top of each other). The second rate constant, k_2, is independent of ATP concentration, but strongly force-dependent, increasing significantly when forward force is applied rather than backward force. This result shows that the force-dependence of motor activity can be at least partially uncoupled from the mechanism of energy utilization. (Adapted from T. J. Purcell *et al.*, Proc. Nat. Acad. Sci., 102:13873, 2005.)

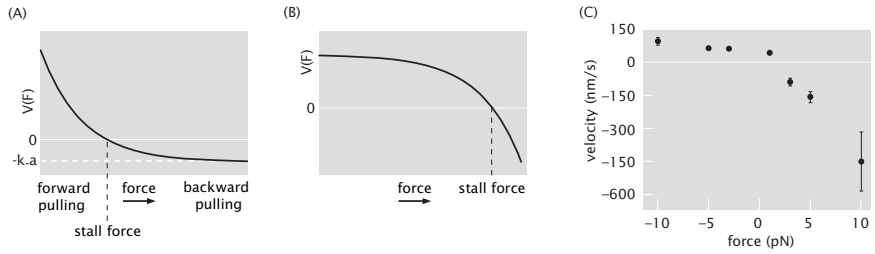

Figure 16.26: Molecular motor velocity as a function of applied force. (A) Theoretical result assuming force-dependence in the forward rate. (B) Theoretical result assuming force-dependence in the backward rate. (C) Data for myosin V, where negative forces represent forward pulling and positive forces represent backward pulling. The shape of the curve most closely resembles the curve in part (B), which would be interpreted in the simple one-state model as indicating that the effects of force on this motor result in changes in the backward rate, not the forward rate. (C, adapted from J. C. Gebhardt *et al.*, Proc. Nat. Acad. Sci., 103:8680, 2006.)

case studies in which the applied force is present in different parts of the rates. As our first example, we assume that all the dependence of the force is in k_+. This means that

$$k_+(F) = k_- e^{-\beta(\Delta G + Fa)} \tag{16.20}$$

which can be plugged into eqn. 16.7 to obtain

$$V(F) = ak_-(e^{-\beta(\Delta G + Fa)} - 1). \tag{16.21}$$

This result is shown in fig. 16.26(A). A second case study is built around the idea that k_+ is independent of the force, assigning all the force dependence to k_- and resulting in

$$k_-(F) = k_+ e^{\beta(\Delta G + Fa)} \tag{16.22}$$

which implies in turn that

$$V(F) = ak_+(1 - e^{\beta(\Delta G + Fa)}). \tag{16.23}$$

This result is shown in fig. 16.26(B). In both cases, if the force is large enough, the motor will start moving backwards. Backward stepping under large applied forces has been directly observed for both myosin V and kinesin. Data from an experiment measuring velocity as a function of applied force for myosin V are shown in fig. 16.26(C) revealing a trend more consistent with the version of the model in which the force primarily influences the magnitude of k_-. However, the reader should bear in mind that this simple one-state model is primarily aimed to illustrate a style of analysis rather than to convey molecular realism consistent with translational motors such as myosin V and kinesin.

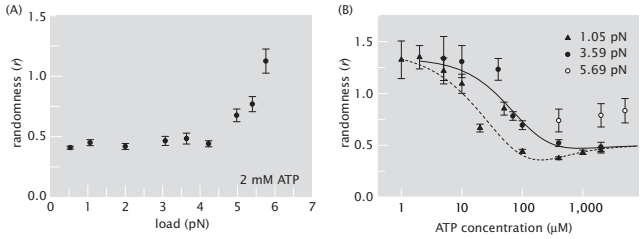

Figure 16.27: Randomness parameter measured for kinesin under a variety of conditions. (A) At high (saturating) concentrations of ATP, the randomness is generally low, indicating that the motor moves at a fairly constant speed. When the load force is very high, approaching the stall force, randomness increases. (B) Randomness also increases at very low levels of ATP (i.e. when the binding rate of ATP may become rate-limiting), and there is a complex relationship between force and randomness at low ATP concentrations, again with higher forces causing higher randomness, or more variability in motor speed. Although this data cannot be fit by a simple one-state model like that described in the text, models invoking more internal states do a better job of accounting for the measurements. (Adapted from K. Visscher *et al.*, Nature, 400:184, 1999.)

In addition to the force dependence of the velocity, this model can help us begin to think about another important experimental parameter called the randomness as well. If we introduce a characteristic time $\tau = a/V$ we can ask what is the diffusive excursion, $\Delta x^2 = 2D\tau = \frac{2Da}{V}$, over that time. The randomness is defined as

$$\text{randomness} = r \equiv \frac{\Delta x^2}{a^2} = \frac{2D}{Va} = \frac{k_+(F) + k_-(F)}{k_+(F) - k_-(F)}, \tag{16.24}$$

where the actual final formula relating the randomness to the rate constants is only valid for the one-state motor we are considering in this model. Note that if $k_+ = k_0[ATP]$, then the randomness will approach one as the ATP concentration gets large. It is more difficult to accurately measure the randomness parameter than it is to measure speed, but nevertheless some data is available. Fig. 16.27 shows one such set of measurements for kinesin. In this case, the experimental results are more subtle than can be captured by the simple one-state model, but are fit reasonably well by a more realistic two-state model, which we will develop below. The problems at the end of the chapter present another opportunity to explore randomness within the one-state model.

16.2.3 Motor stepping from a free energy perspective

So far we have made use of a master equation approach whereby the motor motion is described as a random walk along the filament. The rates k_+ and k_- describe the probability of the motor stepping a distance a to the right, or

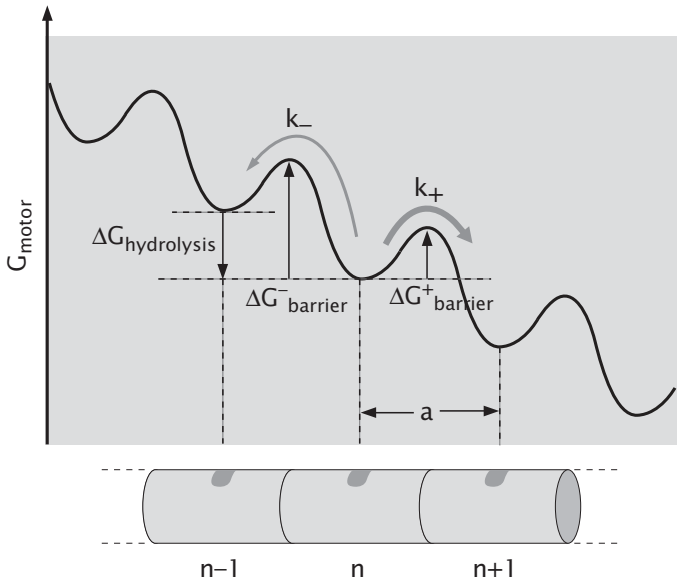

Figure 16.28: The free energy of a motor moving along a filament. n labels the discrete positions of the motor on the filament. The overall tilt of the free energy surface leads to motion of the motor with an average speed to the right. The forward and backward rates are determined by the free energy barriers between the n and $n+1$ state.

to the left, in unit time. An alternative view is provided by the model which depicts the molecular motor as diffusing on a free energy landscape, as shown in fig. 16.28. In this case the rate k_+ can be computed as the inverse average time for the motor to diffuse over the barrier from the nth to the $n+1$st site on the filament, while for k_- the diffusion from $n+1$ to n is the one to consider. Here we make the simplifying assumption that the transition rates are given by the height of the barrier separating the two states via the Arrhenius relation, $k = \Gamma\ exp(-\beta \Delta G_{\rm barrier})$, where Γ is the frequency of attempts to go over the barrier, and $\Delta G_{\rm barrier}$ is the height of the barrier on the free energy landscape.

As in our analysis of the effect of force on motor speed, we can make use of equilibrium arguments to constrain the space of allowed models for the stepping rates k_+ and k_- and how they depend on the concentration of ATP in the toy model of a one-state motor. To begin, we compute the change in free energy associated with a single step of the motor. We assume that each step is accompanied by hydrolysis of a single ATP molecule which in the lattice model shown in fig. 16.29 is represented by having the number of ATP molecules in solution decrease by one, while the number of ADP and P_i increases by one.

If the state that corresponds to the motor being at site n has A ATP molecules in solution, D ADP molecules, and P inorganic phosphates, the sta-

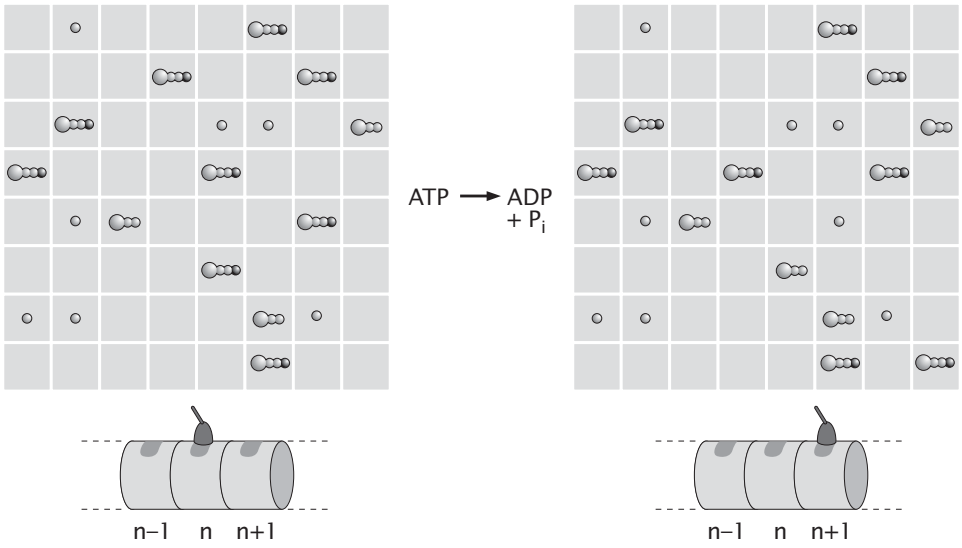

Figure 16.29: Lattice model of motor motility coupled to ATP hydrolysis. Each step of the motor is accompanied by a single hydrolysis event, which decreases the number of ATP molecules by one, and increases the number of ADP and P_i molecules by one.

tistical weight of that state is

$$w_n = \frac{\Omega!}{A!D!P!(\Omega - A - D - P)!}\, e^{-\beta A \epsilon_{\rm bond}} \tag{16.25}$$

where the combinatorial term accounts for all the ways of rearranging the molecules in solution among the Ω boxes, and the Boltzmann factor corresponds to all the bonds between the inorganic phosphate and the ADP present in each of the ATP molecules. Upon hydrolysis the motor moves to the $n+1$ site and one ATP molecule breaks down into an ADP and a Pi. Therefore the statistical weight of this state is

$$w_{n+1} = \frac{\Omega!}{(A-1)!(D+1)!(P+1)!(\Omega - (A-1) - (D+1) - (P+1))!} e^{-\beta(A-1)\epsilon_{\rm bond}} . \tag{16.26}$$

The free energy difference between the state $n+1$ and the state n, which is the free energy of hydrolysis, $\Delta G_{\rm hydrolysis}$, is related to the ratio of the statistical weights for the nth and the $n+1$ state:

$$e^{-\beta \Delta G_{\rm hydrolysis}} = \frac{w_{n+1}}{w_n} = \frac{A}{DP} \Omega\, e^{\beta \epsilon_{\rm bond}} . \tag{16.27}$$

In the last equality we have made the simplifying assumption that the number of boxes in the lattice model is much greater than the number of molecules of

the three species, which are in turn all much bigger than one. Also note that we have rederived from a lattice model perspective the formula for the free energy of ATP hydrolysis (see eqn. 6.122 on pg. 352)

$$\Delta G_{\rm hydrolysis} = \Delta G_0 + k_B T \ln\left(\frac{[D][P]}{[A]} v\right) \tag{16.28}$$

where the concentrations of the different molecular species are given by the number divided by the volume of the solution, Ωv, where v is the volume of a single box. The "standard state free energy" $\Delta G_0 = -\epsilon_{\rm bond}$ in this case corresponds to the energy released upon breaking a single chemical bond in an ATP molecule. The standard state for the lattice model is one where all the boxes are occupied by the three molecular species, i.e. when $[A] = [D] = [P] = 1/v$. (We choose this as the standard state for convenience; biochemists traditionally and arbitrarily use a standard state of 1 M concentration for all chemical species.) Clearly in this state there is no entropy change when a single ATP breaks up into ADP and P_i since there is no freedom for placing these molecules into different boxes, and the free energy of hydrolysis is just the bond breaking energy.

The free energy of hydrolysis we have computed above corresponds to the difference in free energy of successive minima on the free energy landscape on which our motor diffuses and therefore it is equal to the overall slope of the diagram in fig. 16.28. We see that changes in the concentration of ATP, ADP or P_i will lead to a change in the slope of the free energy landscape as required by eqn. 16.28. Hence, within this highly simplified model, the motor velocity will inherit this concentration dependence.

To obtain a formula for how the motor speed depends on ATP concentration, equilibrium considerations are not enough. In the simple model described by the free energy landscape shown in fig. 16.28 we still have to specify how each of the forward rates depends on the ATP concentration. Following our analysis of the effect of force on the motor speed here too we consider two simple scenarios, one in which all the ATP dependence is in the forward rate, and the other where only the backward rate is affected by changing the amount of ATP. The two scenarios are depicted graphically in fig. 16.30.

For the case when only the forward rate is ATP dependent we can use the Arrhenius formula to obtain

$$\begin{aligned} k_+ &= \Gamma_+ e^{-\beta(\Delta G^-_{\rm barrier} + \Delta G_{\rm hydrolysis})} \\ k_- &= \Gamma_- e^{-\beta \Delta G^-_{\rm barrier}} \ . \end{aligned} \tag{16.29}$$

Since the motor speed is $V = a(k_+ - k_-)$, using eqn.16.28 in the above equation for k_+ yields

$$V = a(k_+^0 [A] v - k_-) \tag{16.30}$$

where the rate $k_+^0 = \Gamma_+ e^{-\beta(\Delta G^-_{\rm barrier} + \Delta G_0)} \frac{1}{[D][P]v^2}$ is independent of ATP, and is the forward rate for the standard state concentration of ATP, $[A] = 1/v$. The

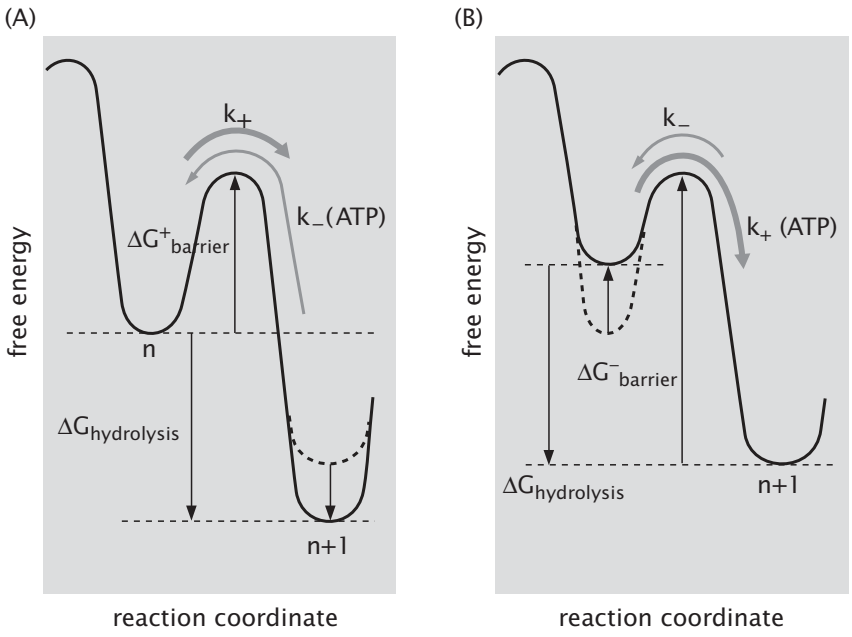

Figure 16.30: Possible scenarios for how the rates depend on the ATP concentration. (A) The backward rate is the ATP-dependent step, while the forward rate is not affected by the concentration of ATP. (B) The forward step is the only one that is ATP-dependent. The dashed line represents the free energy surface for a smaller concentration of ATP and the arrow indicates the change upon increasing the amount of ATP in solution.

prediction is that the speed of the motor increases linearly with ATP concentration. This is clearly contradicted by experiments in the large ATP concentration limit where the motor speed saturates. In fact, the model itself becomes inconsistent for large enough ATP concentrations. Raising the ATP concentration has the effect of decreasing the barrier for stepping from the nth site to the $n+1$ site. When the barrier is gone, i.e. when $\Delta G^{-}_{\rm barrier} + \Delta G_{\rm hydrolysis} = 0$, the Arrhenius form for the transition rate is no longer valid. At best the present model can be used to give an idea of how the motor behaves at concentrations of ATP that are well below saturation.

The case of the backward rate having all the ATP dependence can be analyzed in an analogous way. In this case the rates have the form

$$\begin{aligned} k_+ &= \Gamma_+ e^{-\beta \Delta G^{+}_{\rm barrier}} \\ k_- &= \Gamma_- e^{-\beta (\Delta G^{+}_{\rm barrier} - \Delta G_{\rm hydrolysis})} \ , \end{aligned} \tag{16.31}$$

and the speed of the motor is described by

$$V = a \left(k_+ - \frac{k^0_-}{[A]v} \right) \ , \tag{16.32}$$

where $k^0_- = \Gamma_- e^{-\beta(\Delta G^{+}_{\rm barrier} - \Delta G_0)} [D][P] v^2$. This model does predict saturation of the motor speed at large ATP concentrations, but as is the case of the previous model for high ATP concentrations, at low enough ATP concentrations the barrier for a backward step vanishes rendering the Arrhenius formula meaningless.

The predictions for the dependence of motor speed as a function of ATP concentration for the two models described above are shown in fig. 16.31. They lack the nuance to respond to the full range of experimental data. Still, the one-state motor provides a good starting point for building intuition about the nature of motor dynamics. To actually make convincing contact with experimental data on motors like kinesin, in the next section we begin to analyze a two-state motor.

16.2.4 The Two-state model

The most immediate generalization of the model presented in the previous section is to consider the case in which there are two internal states associated with each position. A schematic description of this model is shown in fig. 16.32. We adopt the indices 0 and 1 to characterize the internal states. An interesting feature of the two-state model, which is different from the one-state picture, is that some of the allowed transitions are not associated with geometric displacements along the filament, but rather, refer to internal transitions such as those involving hydrolysis. For real molecular motors, the internal conformational transitions associated with ATP hydrolysis are coupled to a protein conformational change that generates a single step along the substrate and also to a change in the affinity of the motor head for its substrate. The coupled cycles of

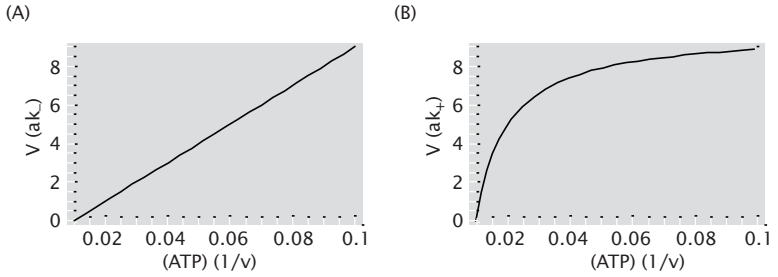

Figure 16.31: Speed of a molecular motor as a function of the ATP concentration as predicted by the one-state model. (A) All the dependence in ATP concentration is in the forward stepping rate. (B) The backward step is ATP dependent while the forward step is not.

binding, ATP hydrolysis, stepping, and unbinding generate directed movement. In the one-state model we were forced to make the non-physical assumption that the forward and backward rate constants were different from one another even though the internal state of the motor was unchanged regardless of the stepping direction; we are now prepared to render the model more realistic (and, as we will see, surprisingly powerful in its ability to make quantitative predictions) by incorporating the second state.

The Dynamics of a Two-State Motor Is Described By Two Coupled Rate Equations

As with our analysis of the one-state motor, our ambition is to write a set of rate equations that describe the time evolution of the probability distribution $p_i(n,t)$ where the label i refers to the internal state (either 0 or 1) and n refers to the position on the linear track. For example, if we interest ourselves in $p_0(n,t)$, we need to consider several different processes that result in the motor being at time t in state 0 at site n. In particular, the motor can come into this state from state 1 at position $n-1$ with a rate k_A^+. In addition, we need to consider the processes in which the motor arrives in this state from state 1 at position n with a rate k_B^-. Finally, there is the uneventful situation where the motor stays put and remains in state 0 at position n during the time interval from t to $t+\Delta t$. This last microtrajectory occurs with probability $1-(k_A^- - k_B^+)\Delta t$.

Following a strategy similar to that we used in the case of the one-state motor, we can write the time evolution of $p_0(n,t)$ as

$$\frac{dp_0(n,t)}{dt} = k_A^+\, p_1(n-1,t) + k_B^-\, p_1(n,t) - k_A^-\, p_0(n,t) - k_B^+\, p_0(n,t). \quad (16.33)$$

Similar reasoning applies to the equation for the time evolution of $p_1(n,t)$ which can be written as

$$\frac{dp_1(n,t)}{dt} = k_A^-\, p_0(n+1,t) + k_B^+\, p_0(n,t) - k_A^+\, p_1(n,t) - k_B^-\, p_1(n,t). \quad (16.34)$$

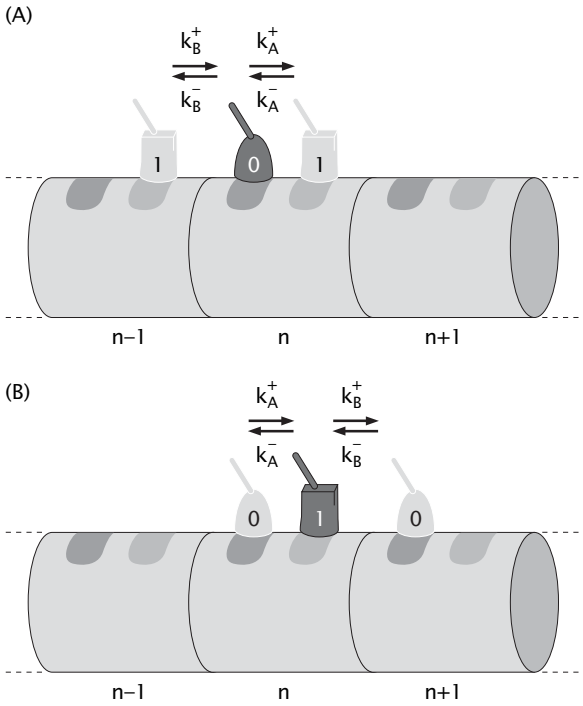

Figure 16.32: Two-state motor model. (A) The rates for the transitions that can occur to change the occupancy of internal state 0. The dark icon indicates the current state of the motor head and the two light icons indicate the two possible states in the next time step. In the two-state model, the motor head is constrained to convert from internal state 0 to internal state 1. This can occur either while the motor remains stationary with respect to the filament (with rate constant k_A) or while the motor takes a single step backwards (with rate constant k_B) (B) The rates for the transitions that can occur to change the occupancy of internal state 1. The motor head can convert to internal state 0, either while remaining in place, or while taking a single step forward.

We are interested in the position of the motor as a function of time which we now derive using certain general observations about the problem.

Though we do not want to enter into the details of how to fully solve models such as the two-state model presented above and we leave this as a homework problem, there is a clever and simple scheme for deducing the velocity in such a model. The trick is to introduce the probabilities P_0 and P_1, which are the probabilities that the motor will be at any site n, but in state 0 or state 1, respectively. That is, we ignore the question of which site the motor occupies and only concern ourselves with its internal state. As a result, we have effectively mapped our problem onto a two-state problem. We can immediately write down the rate equations that capture the dynamics of this two state system as

$$\frac{dP_0}{dt} = k_A^+ P_1 + k_B^- P_1 - k_A^- P_0 - k_B^+ P_0, \tag{16.35}$$

and

$$\frac{dP_1}{dt} = k_A^- P_0 + k_B^+ P_0 - k_A^+ P_1 - k_B^- P_1. \tag{16.36}$$

These two equations can be obtained directly from eqn. 16.33 and eqn. 16.34 by summing both sides over all the sites $n = 1$ to ∞. (For this to make mathematical sense we should make the additional assumption that the motor is moving along a microtubule that is infinitely long.) In steady state, we see that

$$(k_A^+ + k_B^-)P_1 = (k_A^- + k_B^+)P_0. \tag{16.37}$$

A second condition on our probabilities is that the motor be either in state 0 or state 1, which stated mathematically is

$$P_0 + P_1 = 1. \tag{16.38}$$

These two conditions can be used to determine P_0 and P_1 themselves as

$$P_0 = \frac{k_A^+ + k_B^-}{k_A^- + k_B^- + k_A^+ + k_B^+}, \tag{16.39}$$

and

$$P_1 = \frac{k_A^- + k_B^+}{k_A^- + k_B^- + k_A^+ + k_B^+}. \tag{16.40}$$

Given these probabilities, we can now compute the motor velocity by examining the motions implied by each of the possible $0 \rightarrow 1$ and $1 \rightarrow 0$ transitions. For concreteness, we assume that in going from state 0 to 1 at a given site, the distance traveled by the motor is δ and in going from state 1 at one site to state 0 at the next site, the distance moved by the motor is $a - \delta$, where a is the periodicity of the cytoskeletal filament on which the motor moves.

The basic picture is that during each time interval Δt, there are four possible transitions the system can make - a step to the right or the left of length δ can be made by the transition between the 0 and 1 states on the same site, or

alternatively, a step of length $a - \delta$ can be made to the right or to the left by transitions between states 1 and 0 on different sites of the filament. The net result is that the average velocity is given by

$$V = \delta(P_0 k_B^+ - P_1 k_B^-) + (a - \delta)(P_1 k_A^+ - P_0 k_A^-). \tag{16.41}$$

If we now use the results for P_0 and P_1 given in eqns. 16.39 and 16.40, the velocity may be rewritten simply as

$$\langle V \rangle = a \frac{k_A^+ k_B^+ - k_A^- k_B^-}{k_A^- + k_B^- + k_A^+ + k_B^+}. \tag{16.42}$$

An interesting outcome is that the average velocity does not depend on the change in position of the motor (characterized by δ) as it transitions between the two internal states on the same site.

Note that we can rewrite the motor velocity in much the same way that we did for the one-state motor, $V = a(k_+(F) - k_-(F))$, but with the definitions

$$k_+(F) = \frac{k_A^+ k_B^+}{k_A^+ + k_B^+ + k_A^- + k_B^-} \tag{16.43}$$

and

$$k_-(F) = \frac{k_A^- k_B^-}{k_A^+ + k_B^+ + k_A^- + k_B^-}. \tag{16.44}$$

A more detailed analysis of the eqns. 16.33 and 16.34, which is left to the reader as a homework problem, reveals that the diffusion constant for the motor in the two-state model is given by an equation analogous to the one derived for the one-state model, $D = (a^2/2)(k_+(F) + k_-(F))$, with the effective rates as given above.

Models with two or more internal states are more adept at responding to experimental data than the one-state model introduced earlier. An example of the kind of data that has been experimentally measured for kinesin is shown in fig. 16.33. In these experiments, the speed of kinesin-driven movement was carefully measured over a range of ATP concentrations and load forces. The speed of the motor increases when more ATP is present, approaching a constant rate at very high concentrations of ATP. This is reminiscent of the turnover rates of enzymes behaving with Michaelis-Menten kinetics (see fig. 16.53 on pg. 897). For kinesin, the motor speed can be assumed to be proportional to the ATPase enzyme turnover rate, because individual motor steps are uniform in size and are tightly coupled to ATP hydrolysis. Performing the same experiment under different applied loads reveals that increasing the load not only decreases the maximum speed that can be achieved by the motor, but also increases the apparent binding constant of ATP for the motor (that is, the ATP concentration at which the speed is one-half of its maximum value).

Internal States Reveal Themselves in the Form of the Waiting Time Distribution

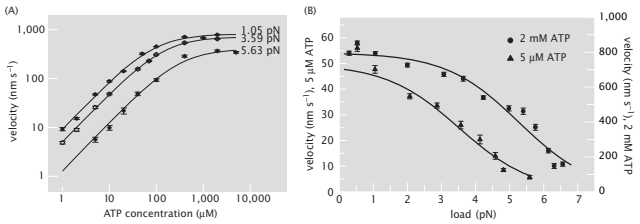

Figure 16.33: Speed of kinesin motors varying with ATP concentration and applied force. (A) Kinesin speed increases with increasing ATP at low concentrations and saturates at high concentrations. (B) Load dependence of motor velocity for several ATP concentrations. (Adapted from K. Visscher *et al.*, Nature, 400:184, 1999; and M. J. Schnitzer *et al.*, Nat. Cell Biol., 2:718, 2000.)

The two-state motor involves internal states which are characteristic of any general treatment of motor dynamics. Some recent experiments have suggested the existence of multiple substates for movements of real molecular motors. Even in cases where we are not able to resolve the internal states in a direct manner there are still some indirect consequences of their existence. One of the most immediate ways in which these internal states reveal themselves is through the waiting time distribution which provides a measure of the pauses between forward steps of the motor. To show how these internal states alter the waiting time distribution, we will consider the case in which each substate has a characteristic lifetime τ_i. This implies that the composite process resulting in net translation of the motor is going to be related to some combination of these times.

Our maximum entropy analysis from chap. 15 showed that the probability density function for waiting times given some average waiting time $\langle t \rangle$ is of the form

$$p(t) = \frac{1}{\langle t \rangle} e^{-t/\langle t \rangle}. \tag{16.45}$$

Recall that this distribution emerges as a result of the constraint

$$\langle t \rangle = \int_0^\infty t\, p(t)\, dt. \tag{16.46}$$

In order to determine the waiting time distribution for a composite process built up of two subprocesses both of which are characterized by exponential waiting times such as in eqn. 16.45, the net waiting time distribution is obtained as

$$p(t) = \int_0^t p_A(\tau)\, p_B(t-\tau)\, d\tau. \tag{16.47}$$

$p_A(\tau)$ is the probability that the first step occurs after time τ and $p_B(t-\tau)$ is the probability that the second step occurs after time $t-\tau$. $p(t)$ is the probability of a total waiting time for the composite process. The integral written in eqn. 16.47

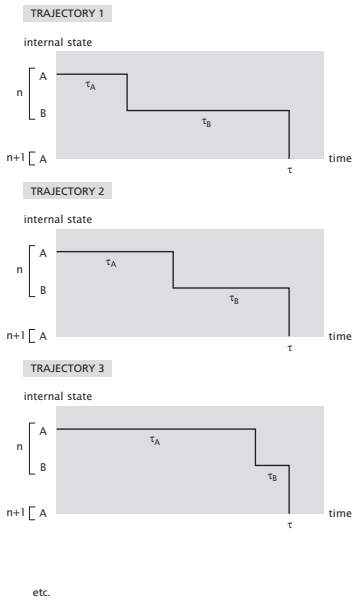

Figure 16.34: Trajectories for a two-state system. The total time to make the two transitions is τ. There are many different ways that the system can make the two transitions during this time τ. There is a waiting time τ_A to make the first step and τ_B to make the second step.

represents a sum over the set of *all* allowed microtrajectories. For example, if $t = 5$ sec, then the integral is a sum over all those intermediate steps whose waiting times add up to a total of 5 seconds. In the case when taking $\tau = 2$ seconds for process A, this implies process B will take 3 seconds. Examples of different allowed composite microtrajectories are shown in fig. 16.34.

We already know the probabilities for the separate subprocesses which can be written in the form

$$p_A(t) = \tau_A^{-1} e^{-t/\tau_A} \tag{16.48}$$

and

$$p_B(t) = \tau_B^{-1} e^{-t/\tau_B}. \tag{16.49}$$

As a result, eqn. 16.47 can be written explicitly as

$$p(t) = \int_0^t e^{-\tau/\tau_A} e^{-(t-\tau)/\tau_B} \, d\tau \frac{1}{\tau_A \tau_B}. \tag{16.50}$$

This integral can be evaluated (assigned as a problem at the end of the chapter) and results in

$$p(t) = \frac{1}{\tau_B - \tau_A} \left(e^{-t/\tau_B} - e^{-t/\tau_A} \right) \tag{16.51}$$

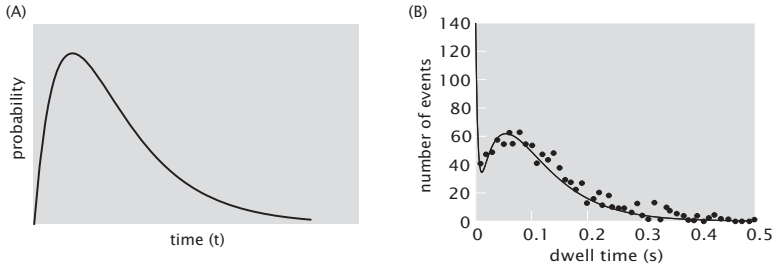

Figure 16.35: Probability distribution for waiting times for a two-state motor. (A) Theoretical result, as stated in eqn. 16.51. (B) Data on dwell time distribution for a single-headed version of myosin V, at 10 μM ATP. (Adapted from Purcell et al., 2005, and J. C. Liao *et al.*, Proc. Nat. Acad. Sci., 104:3171, 2007.)

Fig. 16.35 shows the functional form of this class of waiting time distribution. In practice, observed dwell times for various molecular motors fit well to this kind of scheme.

Because the rates of internal conformational changes for motors in position-state models depend on nucleotide hydrolysis state and on applied force, we expect that dwell time distributions should also depend on these factors. Fig. 16.36 shows average dwell times for myosin V as a function of force for two different concentrations of ATP. At high ATP, dwell times are initially very short, but increase with load as the motor is forced to do more work. At very low concentrations of ATP, the behavior of the motor is dominated by the state while it is waiting for a nucleotide to bind, and is less sharply dependent on applied force. The conclusion of this analysis is that the overall distribution of dwell times provides a window on the composite processes that make up the overall motor dynamics and a filter on the different classes of models set forth to greet data on dwell times.

16.2.5 More General Motor Models

In general, the internal dynamics of molecular motors can be considerably more complex than the one- and two-state motors considered thus far. The P-state, N-position class of models introduced in fig. 16.19 is probably still a useful framework for thinking about these motors. For example, in order to fit all the data available for kinesin, it appears that a model based upon four internal states is most realistic. The complexity of the mathematics and the proliferation of parameters makes these models largely beyond the scope of this book. However, before turning to other classes of motors besides the translational motors considered here, we first make some general observations.

As an example of the proliferation of internal states consider the particular case of myosin shown in fig. 16.37. This figure schematizes the various subpro-

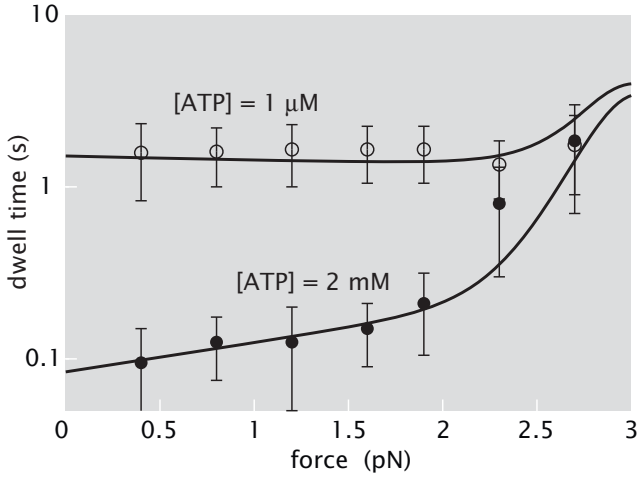

Figure 16.36: Average dwell times for myosin V as a function of load, for high ATP (solid circles) and low ATP (open circles). The lines represent a fit of the data to a two-state model. (Adapted from A. D. Mehta *et al.*, Nature, 400:590, 1999 and A. B. Kolomeisky and M. E. Fisher, Biophys. J., 84:1642, 2003.)

cesses present in the cycle of a myosin molecule as it moves along actin. In the first stage, a myosin head is bound to an actin filament (attached), from which it unbinds upon ATP binding allowing it to move along the filament (released). ATP gets hydrolyzed (the resulting ADP and phosphate remain bound) producing a larger conformational change, which causes the head to be displaced around 5 nm along the filament (cocked). The phosphate gets released in order to bind the head to the new position on the filament and the power stroke starts, during which the ADP molecule gets released (force-generating) returning to the initial stage. The argument is that each of the internal states exhibited by myosin can be represented in the framework introduced above, but now with further internal states per geometric position.

There are a number of different experimental dials that can be controlled to elicit different motor responses. Two of the most interesting ways to perturb the dynamics of molecular motors like myosin and kinesin are to change the ATP concentration and to apply forces to the motor, as we have seen in several cases above. Another particularly interesting kind of perturbation is to link several individual motors so that they are forced to work together. We now turn to this fascinating topic.

16.2.6 Coordination of Motor Protein Activity

Thus far we have focused on the remarkable mechanical properties of individual motor molecules. Nevertheless, in cells it is rare for a single molecule to accom-

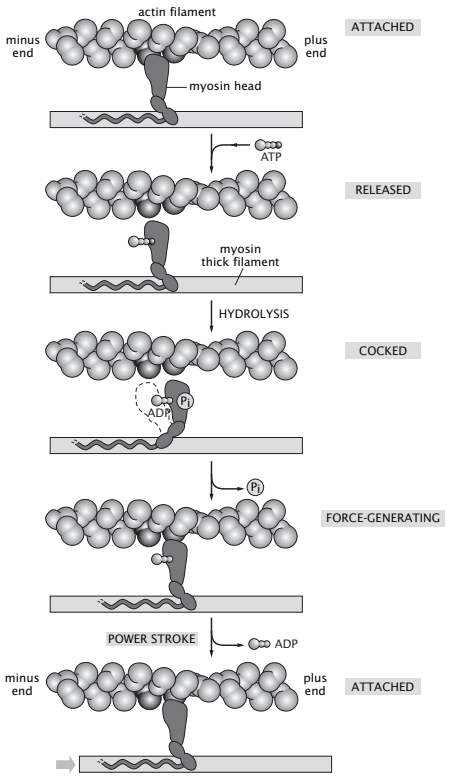

Figure 16.37: Model of myosin walking on an actin filament in a muscle. Actin thin filaments and myosin thick filaments are arranged in a regular array in muscle such that individual myosin heads protruding from the thick filaments are conveniently positioned to step along the actin filament tracks. At the beginning of a single step cycle, the myosin motor head domain is attached to the actin filament. Binding of ATP to the myosin releases it. ATP hydrolysis is coupled to a conformational change such that the head is poised over the next subunit on the actin filament. When phosphate is released from the myosin head it is able to bind in this new position. Release of ADP from the myosin head is coupled to the force-generating power stroke. (Adapted from B. Alberts *et al.*, Molecular Biology of the Cell, 4th ed. New York: Garland Science, 2002.)

plish anything notable on its own. More typically, the action of many individual motors must be coordinated to achieve a larger scale goal. An impressive example of this is seen in muscle fibers where the 10^{14} heads (as estimated in section 16.1) must all cooperate and generate force nearly simultaneously without interfering with one another. These concerted motor motions generate the macroscopic shortening of the muscle that enables us to run, jump and swim. How is this coordination achieved?

There are three requirements for motor coordination during muscle contraction: first, that all acting motor heads move in the same direction; second, that they all generate force at the same time; and third, that they not interfere with one another. In muscle, the first requirement is achieved by the exquisite geometrical control exercised by cells during the development of the sarcomere as shown in fig. 16.7. The second is achieved through the action of a group of actin binding proteins called tropomyosin and the troponins whose choreographed response to calcium signals is shown in fig. 16.38. The long tropomyosin protein physically prevents binding of the myosin heads to the actin filaments so that contraction can only occur in response to a positive signal, the influx of calcium into the cell. Because calcium ions flood the entire cell extremely rapidly as a consequence of the rapid propagation of membrane depolarization (which will be discussed in chap. 17), the tropomyosin block can be removed nearly simultaneously throughout the entire muscle cell, thus enabling large-scale coordinated contraction. The third requirement is alleviated by the fact that an individual myosin head in a skeletal muscle remains tightly bound to the actin filament for only a short fraction of the time of its ATPase cycle (less than 5 percent). Thus, one head generates a power stroke and rapidly detaches so as not to interfere with the action of other heads. Tellingly, this feature is not true for motor proteins such as myosin V or kinesin that have to work processively on their own; these motor heads remain tightly bound for more than 50 percent of their ATPase cycle.

Muscle is a special case, where evolution has resulted in a system where motor head behavior can be coordinated for millions of individual molecules throughout an entire cell. More commonly, it is smaller teams of motors that need to work together. For the two-headed processive motors such as myosin V and kinesin, it is important that the rear head not release from the filament until the front head is firmly bound. Otherwise, the motor and its attached cargo would be at risk of drifting away due to thermal motion, which is significant at molecular distance scales. Thus, the two heads must somehow communicate through their linked domains to influence one another's cycles of ATP hydrolysis and filament binding. The mechanisms of this form of molecular communication are currently under investigation. One interesting approach to this problem is illustrated in fig. 16.39. In this experiment, protein engineering was used to create a series of artifically oligomerized kinesin motor heads, linked by a series of rigid rod-shaped protein domains and elastic spring-like protein domains. While individual kinesin heads were able to generate microtubule gliding at reasonable rates, linked pairs and triplets were able to cooperate to generate progressively faster motion. Cooperation was manifested even by these artificially engineered

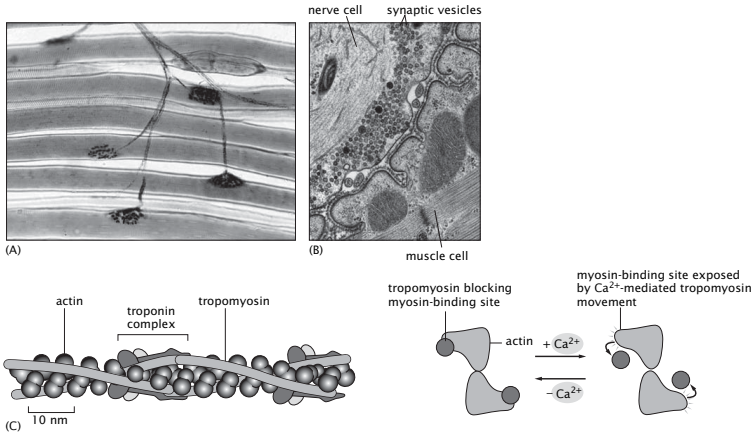

Figure 16.38: Schematic of coordination in muscle contraction. (A) A bundle of muscle fibers is innervated by a single motor neuron which forms communication synapses with all the fibers in the bundle. (B) At each of these synapses a differentiated portion of the nerve terminal is stuffed with acetylcholine containing vesicles lined up across the intercellular gap from their target muscle cell. After the neuron releases its neurotransmitters, acetylcholine binding to receptors on the muscle cell triggers a nearly instantaneous influx of calcium ions throughout the entire cytoplasm of the giant muscle cell. (C) In the resting muscle cell, myosin heads are prevented from binding to the actin filaments because the actin is coated with a series of copies of a long, skinny protein called tropomyosin, which is also associated with several small calcium-binding proteins called troponins. When calcium ions bind to troponin, a conformational change causes tropomyosin to shift its position on the actin filament revealing the myosin binding sites which can then be simultaneously attacked by the myosin motor heads poised nearby. (A, courtesy of Thomas Caceci ; B, courtesy of John Heuser; C, adapted from B. Alberts *et al.*, Molecular Biology of the Cell, 4th ed. New York: Garland Science, 2002.))

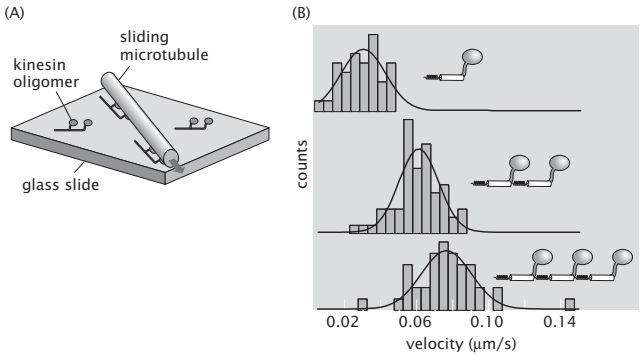

Figure 16.39: Cooperation among linked motors. (A) Schematic of the experiment, showing immobilized kinesin oligomers moving microtubules in a gliding assay. (B) Speed measurement histograms for individual microtubules being moved on slides coated with either single kinesin heads (top), linked pairs of kinesin heads (middle), or linked triplets of kinesin heads (bottom). Although the individual molecular motor head units are identical in each case, coupling multiple heads together enables them to generate faster gliding speeds. (Adapted from M. R. Diehl *et al.*, Science, 311:1468, 2006.)

protein constructs, where the molecular structure of the links between the motor heads bears no resemblance to the links found in any real molecular motors. This result provides hope that the mechanisms of cooperation between linked heads can perhaps be understood in purely mechanical terms.

Frequently, it is necessary for multiple copies of different kinds of motors to work together, for example in the intracellular transport of membrane-bound organelles and vesicles. One example of this kind of transport is shown in fig. 16.40. These cells, melanocytes, contain many small vesicles filled with dark pigment called melanosomes. In some fish and amphibians, the cells can change colors in response to hormonal signals, communicating when the animal is frightened, angry or sexually aroused. This is accomplished by virtue of the fact that each melanosome is coated with three different types of motor protein, a dynein motor that moves the melanosomes inwards towards the center of the cell along microtubule tracks, a kinesin motor that moves in the opposite direction along the same track, and a myosin V motor that moves along actin filaments at the cell periphery. Strikingly, when a cell receives a hormonal signal, all the melanosomes in the cell switch directions simultaneously. This is because the hormonal signals indirectly induce phosphorylation of proteins that regulate the motors' activity such that either the inward motor or the outward motor predominates. The examination of coordinated motor activities is one of the exciting current frontiers in motor research.

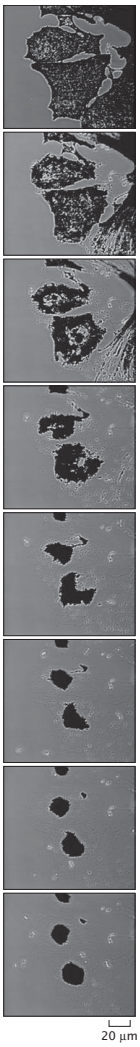

Figure 16.40: Transport of pigment granules. Pigment cells cultured from the skin of a black tetra reorganize their pigment granules after stimulation with adrenaline. Frames shown from a video sequence are separated by approximately two minute intervals. The aggregation of the pigment granules in the center of the cell makes the fish appear to change to a lighter color. (Adapted from V. I. Rodionov and G. G. Borisy, Nature, 386:170, 1997.)

16.2.7 Rotary Motors

Throughout the preceding section we have developed the idea of position-state models for translational motors imagining that each energy requiring step is coupled to the movement of a motor along a linear track. This same formalism can easily be generalized to the second major biological class of motors, the rotary motors, by imagining the track bent into a closed circle. As illustrated in fig. 16.15, rotary motors also move in a series of discrete steps with each rotational step is tightly coupled to an energy releasing reaction. These are typically either the hydrolysis of ATP or the transport of an ion across a membrane down an electrochemical gradient.

Important mechanical quantities introduced to describe translational motors all have direct analogs in the rotational motor setting. For example, linear speed in the translational context becomes angular velocity in rotary motors, the force generated becomes torque. An interesting question to consider then is: how is the angular velocity of a rotary motor related to the applied torque, and how does it depend on the available energy (i.e. ATP concentration or electrochemical potential)?

As shown in fig. 16.41, rotary motors are typically large, multiprotein machines with a series of similar subunits arranged in a ring. In the example illustrated in this figure, the transport of a single sodium ion across the membrane is accompanied by a conformational change in the motor that is equivalent to a single step of the moving ring (called the rotor) with respect to a complementary immobile unit (called the stator).

The motor is driven by thermal fluctuations which result in rotational diffusion of the rotor. Diffusion of the rotor is rectified, leading to directed motion, by electrostatic interactions between the charges on the rotor, the stator, and the Na ions. Specifically, the rotor charge is captured by the stator charge, which is of opposite sign. The captured rotor charge can then diffuse away from the stator charge until it finds itself in the input channel (fig. 16.41), where it is exposed to a large concentration of Na^+ ions on the periplasmic side. The rotor charge can then capture a Na^+ atom from the periplasm rendering it partially neutral, which allows it to diffuse away from the stator charge. Once it leaves the stator, the Na^+ ion is released on the low-concentration cytoplasmic side. The driving force leading to the rotation of the motor is thus the free energy difference experienced by the Na^+ ion as it travels from the periplasmic to the cytoplasmic side.

This type of mechanism applies to torque generation by both the bacterial flagellar rotor and the F_0 subunit of ATP synthase. In the case of ATP synthase, we have an interesting opportunity to compare torque generation by ion transport (for F_0) and torque generation by ATP hydrolysis (for F_1).

- **Estimate: Competition in the ATP Synthase.** One of the remarkable features of the ATP synthase is that it can rotate in either direction depending upon the magnitude of the ion gradient across the membrane and upon the concentrations of ATP, ADP and P_i. In this estimate, our

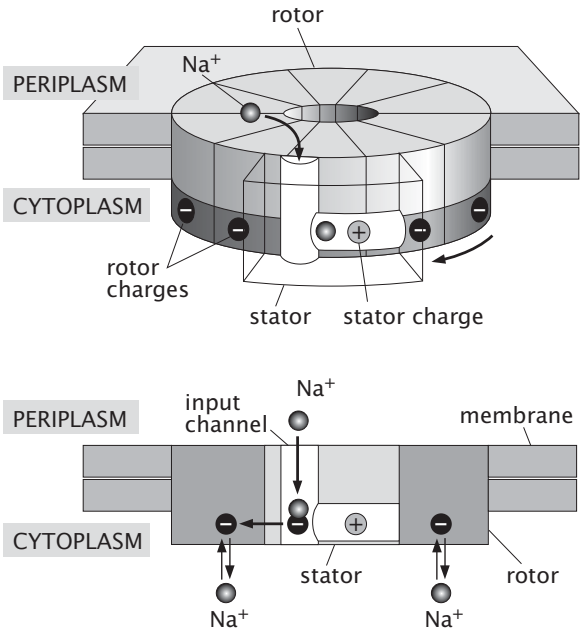

Figure 16.41: Operation of a sodium ion transporter. Diagram of the F_0 motor from the bacterium *Propionigenium modestum*. While the F_0 of most bacteria transports hydrogen ions, this interesting example uses sodium ions instead. The movement of a single sodium ion through the rotor requires a turn of one step to bring the partially transported ion into registry with the charge distribution in the stator ring. At any given moment, no direct channel between the periplasm and the cytoplasm exists, but ions still move across the membrane. They enter from the periplasm when the rotor is in one position and exits into the cytoplasm when the rotor has turned by one step. This leads to rotational diffusion with drift, of the rotor. (Adapted from C. Bustamante *et al.*, Acc. Chem. Res., 34:412, 2001.)

interest is in examining the magnitude of the torque that can be applied in each of the two directions. In particular, the F_0 unit can be induced to rotate as a result of an ion flux across the membrane, with a thirty degree rotation resulting from each ion transported. By way of contrast, the F_1 subunit rotates as a result of ATP hydrolysis with a 120 degree rotation for each ATP hydrolyzed.

We can estimate the torque produced by the motor in both of these modes of operation by assuming that the entire free energy change associated with ion transport (F_0) or ATP hydrolysis (F_1) can be converted into useful work. The torque is equivalent to the tilt of the free energy landscape on which the motor diffuses, and as such serves as the driving force for directed rotational motion, directly analogous to the way that applied force tilts the free energy landscape for a linear translation motor For F_0, we can write

$$\Delta G_{tot} = \Delta G_{pot} + \Delta G_{conc}, \tag{16.52}$$

where ΔG_{pot} is the free energy change associated with moving an ion across the transmembrane electrical potential and ΔG_{conc} is the free energy change associated with the change in entropy corresponding to taking the charge at a concentration c_{out} and moving it to a region with concentration c_{in}. The contribution to the free energy resulting from moving the ion across the transmembrane potential is given by

$$\Delta G_{pot} = e\Delta V. \tag{16.53}$$

For a typical membrane potential difference of 90 mV this results in an energy release of roughly 4 k_BT. The entropic contribution to the free energy release associated with taking ions at the concentration outside the cell and installing them inside the cell is given by

$$\Delta G_{conc} = k_BT \ln \frac{c_{out}}{c_{in}}. \tag{16.54}$$

If we assume perfect free energy conversion, this means that the entirety of the free energy difference due to ion transport is available to do work and results in a torque

$$\tau_{F_0} \approx \frac{4\ k_BT}{\pi/6} + \frac{k_BT}{\pi/6}\ \ln\ \frac{c_{out}}{c_{in}} \approx 30 + 20\Delta pH \text{ pN nm}. \tag{16.55}$$

where ΔpH is the difference in pH between the inside and the outside of the cell.

As noted above, the motor can run in reverse if the concentration of ions is sufficiently low and the concentration of ATP is sufficiently high. When running in reverse, the maximum torque that can be generated by F_1 can be estimated as

$$\tau_{F_1} \approx \frac{\Delta G_0}{2\pi/3} + \frac{k_BT}{2\pi/3}\ ln\ \frac{[ADP][P_i]}{[ATP]} \approx 40\text{pN nm} \tag{16.56}$$

where in the last equation we made use of the typical value, $20k_BT$, for the free energy released during a hydrolysis event of a single ATP molecule under physiological conditions.

Comparing the two equations for the torque we see that by tuning ΔpH, one can reverse the direction of the motor. The crossover point occurs at approximately $\Delta pH \approx 0.5$. Healthy *E. coli* normally maintain ΔpH around 0.75, meaning that normally the torque generated by F_0 is stronger and ATP is synthesized. ΔpH can vary from about 2.0 to about -0.25 depending on the pH of the external medium. When the external medium is very alkaline (i.e. pH > 8.0), ATP synthase runs backwards.

16.3 Polymerization and Translocation as Motor Action

16.3.1 The Polymerization Ratchet

Until now, our quantitative discussion of motors has centered on translational motors that move along cytoskeletal tracks. Interestingly, the cytoskeletal filaments that serve as the scaffolding for translational motors themselves exhibit motor action. Indeed, cytoskeletal polymerization is one of the cell's main mechanisms for applying forces in particular places. An interesting model for force-generating polymerization is the polymerization ratchet. The basic idea is that the addition of monomers onto the end of a growing filament can result in a pushing force on some resisting barrier, either by virtue of fluctuations in the position of the barrier or in the position of the filament itself. For concreteness, we can think schematically of growing actin filaments pushing against a cell membrane at the leading edge of a crawling cell.

We begin by thinking of a cytoskeletal filament that has grown to a length such that there is no room between it and the resistive barrier. This kind of experiment was illustrated in fig. 10.33 (pg. 543). Once the cytoskeletal filament has encountered the barrier it appears that there is no room for the next monomer to come in and attach. It would seem that the polymerization process would grind to a halt. However, if the barrier jiggles and a new monomer sneaks in now and then when there is room for it to fit, the net result will be an ever increasing displacement of the membrane. Similarly, the filament itself will fluctuate and might bend away from the barrier so that a new monomer has room to bind. Regardless of the precise mechanism the fluctuation is "frozen" in, leading to the generation of a deforming force that acts on the membrane. The net result is that a growing actin filament will do work against the elastic forces that would like to keep the barrier undeformed.

Based on the ratchet picture described above and using thermodynamic reasoning, we can estimate the maximum force that the growing filament can exert. In the absence of a force, the free energy landscape for monomer addition looks like the schematic shown in fig. 16.42. In the presence of a force, the addition of a new monomer has an additional free energy cost because of the

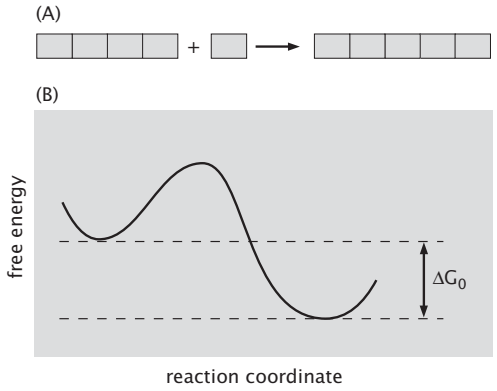

Figure 16.42: Free energy picture of equilibrium polymerization. The addition of each monomer on to the growing filament leads to a decrease in the net free energy of the system. Cells can harness the free energy decrease associated with protein polymerization to do useful mechanical work.

work $F\delta$ that it has to do in the presence of the barrier. This is simply the work that the filament does against the applied force over a distance equal to the length of the monomer. In terms of a free energy diagram, as shown in fig. 16.43 the effect of the force is to raise the free energy of the on state compared to the off state by an amount $F\delta$. This change in the free energy difference between the two states leads to an increase in the dissociation constant for the polymerization reaction,

$$K_d(F) = K_d(0)\exp(F\delta/k_BT). \tag{16.57}$$

As discussed in the previous chapter, the dissociation constant is equal to the monomer concentration m at which the average filament length is not changing in time. Therefore the maximum force that can be generated by the growth of a filament when the monomer concentration is m is given by the relation,

$$m = K_d(0)e^{F_{\max}\delta/k_BT} \ . \tag{16.58}$$

Solving this equation for the maximum force we arrive at,

$$F_{\max} = \frac{k_BT}{\delta}\ln\frac{m}{m^*} \tag{16.59}$$

where $m^* = K_d(0)$ is the critical concentration in the absence of force.

Using this simple formula we can obtain estimates for the maximum force exerted by polymerization of actin and microtubules. Inside of living cells, the concentration of actin monomers is estimated to be $\approx 20\ \mu$M, that is $m = 100m^*$, and the length δ that the filament grows by addition of a single monomer is given by

$$\delta \approx \frac{5.4\text{ nm}}{2\text{ protofilaments}} = 2.7\text{nm} \tag{16.60}$$

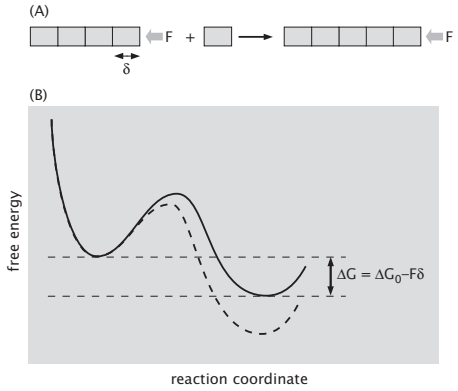

Figure 16.43: Polymerization against a force. The presence of an applied force tilts the free energy landscape and makes the addition of the next monomer less favorable than it would be in the absence of a force.

we get the maximum force as,

$$F_{max} = \frac{4 \text{ pN nm}}{2.7 \text{ nm}} \times \ln 100 \approx 7 \text{ pN}. \tag{16.61}$$

For microtubules, for the sake of an estimate we take excess tubulin concentration $m = 100m^*$ to be on the same order as the excess actin concentration, with a length change contributed by addition of a single monomer given by

$$\delta = \frac{8 \text{ nm}}{13 \text{ protofilaments}} \approx 0.6 \text{ nm}. \tag{16.62}$$

Hence, the critical force is given by

$$F_{max} = \frac{4 \text{ pN nm}}{0.6 \text{ nm}} \times \ln 100 \approx 30 \text{ pN}. \tag{16.63}$$

This result suggest that, all other things being equal, polymerization motors that take smaller unit steps are able to generate larger forces. In real cells, it is sometimes observed that individual growing or shrinking microtubules may exert biologically significant forces, while actin filaments almost always work in groups.

One limiting factor that is not taken into account by the previous estimate is that the maximum force exerted by a polymerizing filament might not be attained if the filament buckles. While the polymerization force generated by a single filament is constant regardless of filament length, longer filaments are more easily buckled than shorter filaments. As we discussed in chap. 10 and derived in eqn. 10.70 (pg. 545), we can estimate the buckling force as

$$F_{\text{buckle}} \approx \frac{k_{\text{flex}}}{L^2} \tag{16.64}$$

where the flexural rigidity of the filament is the parameter that characterizes its resistance to bending, and it is related to its persistence length via $k_{\text{flex}} = \xi_P k_B T$. From this formula we see that k_{flex} has units of Energy $\times$ Length, and therefore we must divide by Length^2 to obtain a force.

Since the buckling force is inversely proportional to the length squared, it is only very short filaments that will be able to sustain a load equal to $F_{\max}$ without buckling. The critical length is determined by setting the two forces equal. For an actin filament with a persistence length of 15 μm, setting $F_{buckle} = F_{max}$ and using eqn. 16.64, yields

$$\frac{4 \text{ pN nm} \cdot 15 \ \mu\text{m}}{L_{\max}^2} = 7 \text{ pN} \tag{16.65}$$

and $L_{\max} \approx 0.1$ μm is the maximum length that can withstand buckling. Arrays of growing actin filaments that need to exert a force inside of cells are usually linked together by crosslinking proteins, forming bundles or networks where the average length of a free filament end is much shorter than this limit, as shown in figs. 14.2 (pg. 716) and 15.3 (pg. 756). We can make the analogous estimate for microtubules, for which $F_{\max} \approx 30$ pN, and which are considerably stiffer than F-actin with a persistence length of 3 mm, to obtain $L_{\max} \approx 0.6$ μm.

The Polymerization Ratchet Is Based on a Polymerization Reaction That Is Maintained Out of Equilibrium.

The thermodynamic arguments put forward above give upper bounds on the size of the force that a growing filament can exert on a load. In order to judge the usefulness of this estimate, as well as gain quantitative intuition about the time scales involved in filament polymerization against a load, we require a dynamical model that can provide an estimate for the length of time that it will take to add each monomer to a growing filament. At a molecular scale, it is likely that thermal motion of some element in the system will be sufficient to open up a monomer-sized space between the end of the filament and the barrier load. The general class of kinetic models that assume thermal motion as a rate-limiting step is commonly referred to as the thermal ratchet or Brownian ratchet model.

A schematic of one form of the Brownian ratchet is shown in fig. 16.44. A polymer made up of monomers of length δ is growing near a load object, such as the cell membrane. Each time thermal fluctuations of the position of the membrane cause the gap between the polymer and the load to be greater than δ, a monomer can attach itself to the growing tip, thereby effectively pushing the load forward. One of the key quantities we wish to compute is the velocity with which the load will move.

In the absence of a force on the load object we can obtain an estimate of its velocity by making two simplifying assumptions: i) once monomers attach they do not fall off, and ii) monomers attach immediately upon appearance of a gap which is larger than the monomer size δ. The time for the load to diffuse over a distance δ can be estimated from its diffusion constant, $t_D = \frac{\delta^2}{2D}$. Using

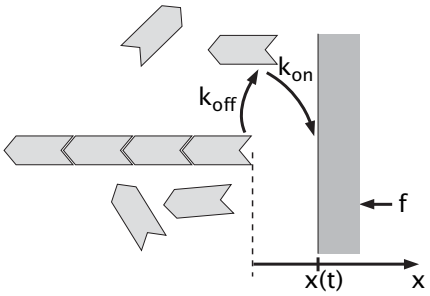

Figure 16.44: Polymerization Brownian ratchet. The growing filament induces a displacement of the obstacle which pushes back with a force f. In this particular model, the barrier is able to move back and forth along the x axis due to thermal fluctuations, occasionally opening up a large enough space for the insertion of a new monomer at the growing tip.

the simplifying assumptions given above, we can estimate the velocity on the grounds that after this time the load will have displaced permanently by an amount δ. Therefore its average ("ideal") velocity is, $v_{id} = \frac{\delta}{t_D}$ and

$$v_{id} = \frac{2D}{\delta}. \tag{16.66}$$

The result is that the ideal velocity of the tip must be proportional to the diffusion constant of the load object.

This idea has been tested experimentally, by using different sizes of bacteria or of polystyrene beads coated with bacterial proteins to generate polymerization-driven actin comet tails such as those shown in fig. 15.3 (pg. 756). Contrary to the predictions of this very simple model, the speed depends only weakly on the size of the load object, and is not proportional to its diffusion coefficient. An alternative model in which the fluctuations of the growing filament itself are responsible for opening up monomer-sized gaps has been proposed to account for this discrepancy, and makes more accurate predictions of how speed depends on varying experimental conditions. A further complication of the real systems compared to this idealized treatment is the influence of other forces on speed, including adhesive forces connecting a subset of the growing actin filaments to the load object. Nevertheless, regardless of details, the basic idea of ratcheting thermal fluctuations of some mechanical element of the system (including the load and the filament tips) by maintaining a non-equilibrium concentration of monomers is a good starting point for building a quantitative model of the polymerization motor.

We can generalize the kinetic model in a way that is applicable to any of these particular implementations of the idea of the Brownian ratchet by calculating the speed in terms of the probability per unit time that a monomer will be added to the growing filament, regardless of the precise physical mechanism

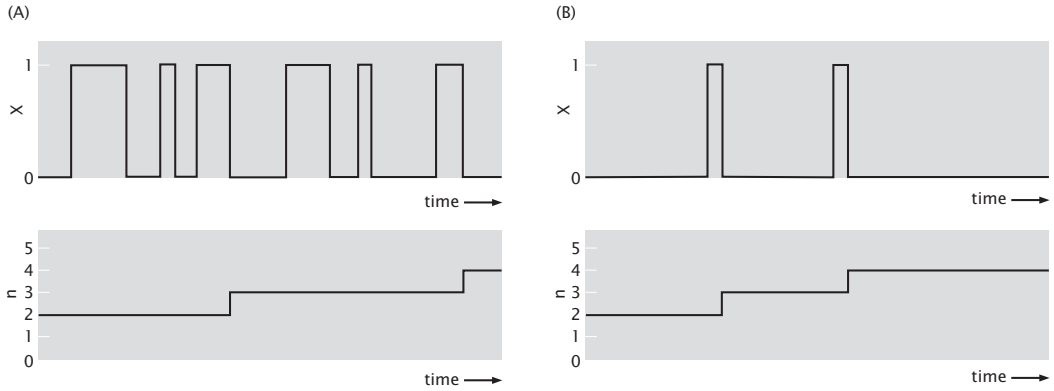

Figure 16.45: Trajectories for the load position (top, X) juxtaposed with polymer length (bottom, n) for the (A) diffusion-limited and (B) reaction-limited regimes of the simple Brownian ratchet. When the elongation reaction is diffusion-limited, the load is frequently in a position favorable for monomer addition, but monomers collide with the filament end comparatively rarely. When the elongation reaction is reaction-limited, the load is rarely in a position favorable for monomer addition, but monomer addition occurs every time it is permitted.

that opens up the space. Here, we need to consider two slightly different kinetic scenarios, illustrated in fig. 16.45. In the first regime, termed diffusion-limited, the rate-limiting step for elongation of a filament is simply the time it takes for a diffusing monomer to accidentally collide with the filament tip. Once a collision has occurred, the monomer quickly becomes incorporated. In the second regime, termed reaction-limited, the incorporation of a monomer into a filament is much rarer than the collision frequency. In either case, the probability that a monomer attaches to a filament in time interval Δt can be written as the probability that an attachment is allowed, times the probability that an attachment will occur *assuming* it is allowed: $\Delta p(\text{on}) = p(\text{allowed}) \times k_{\text{on}} m \Delta t$. In the reaction-limited regime, the probability that an attachment is allowed is equal to the probability that the load position from the edge of the growing filament is greater than δ. In the diffusion-limited regime, the time between attachments is long enough so that the load can sample all possible positions. Therefore, the probability that an attachment is allowed is equal to the *equilibrium* probability that the load position is greater than δ, $p_{\text{eq}}(x > \delta)$. For actin and microtubule polymerization, most experimental work indicates that their growth is likely to be diffusion-limited rather than reaction-limited, even under substantial load forces.

Now we can write the average polymerization rate as

$$v = \delta(k_{\text{on}} m p_{\text{eq}}(x > \delta) - k_{\text{off}}). \tag{16.67}$$

The equilibrium probability that the gap between the polymer and the load is

greater than x is given by,

$$p_{\rm eq}(x > \delta) = \int_{\delta}^{\infty} p_{\rm eq}(x) d\, x \tag{16.68}$$

where

$$p_{\rm eq}(x) = \frac{F}{k_B T} e^{-Fx/k_B T} \tag{16.69}$$

is the equilibrium probability of finding the load at position x away from the growing tip of the filament. Doing the integral in eqn. 16.68 and substituting the result into eqn. 16.67 leads to the expression of the force dependent polymerization rate in the reaction limited regime

$$v = \delta[k_{\rm on} m e^{-F\delta/k_B T} - k_{\rm off}] \ . \tag{16.70}$$

An implicit assumption we have made all along is that the off-rate is not affected by the force. One experimentally testable prediction of the model is the exponential fall-off of the rate on applied force with a characteristic force of $k_B T/\delta$. For microtubules the characteristic force is approximately 7 pN, while the experiments find a corresponding value of roughly 2 pN, which is reasonably good agreement considering the extreme simplifications incorporated in the model. Also, note that the model predicts the maximum force equal to that predicted earlier from equilibrium considerations. At this value of the force the filament switches from growth to shrinkage.

To make further progress, we now switch our attention to the assumption that the reaction time is much less than the diffusion time, another straightforward consequence of working in the diffusion-limited regime. In this case a movie of the growing filament would reveal rapid fluctuations of the filament between states with length n and $n-1$ with the filament in the n state most of the time (this assumes that $k_{\rm on} m > k_{\rm off}$) as shown in fig. 16.45. (One might also observe shorter filament lengths as well but these would require two consecutive events with a monomer falling off the filament, which is considerably less likely than an off event followed by an on event.)

Eventually the movie would show the filament growing to length $n+1$, but this would happen only after the load has had time to diffuse over a distance δ. On the diffusion time scale, the monomer would attach instantaneously, as soon as the load is at a position to allow for the attachment of a new monomer. At this point in time the filament length would begin to fluctuate between length $n+1$ and n. We conclude that in this diffusion limited regime the average filament growth rate would be $1/\tau_1$, where τ_1 is the average time it takes the diffusing load to reach the position δ; this time is also referred to as the first passage time. Computing the first passage time is a classic problem in diffusion theory and here we do it in the simple setting of one-dimensional diffusion.

The Polymerization Ratchet Force-Velocity Can Be Obtained By Solving a Driven Diffusion Equation

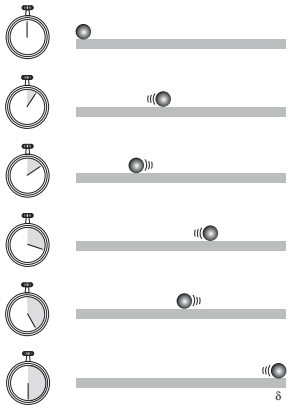

Figure 16.46: Mean time to capture

As a warm-up exercise we compute the first passage time in the absence of a force. We consider the diffusion equation for the steady-state probability $p(x)$ of finding a particle at position x within an interval of width δ as shown in fig. 16.46. We assume that when a particle crosses the $x = \delta$ boundary it disappears and then immediately reappears at $x = 0$. This condition ensures that the probability of finding the particle anywhere in the $(0, \delta)$ interval is equal to one. Furthermore, with this boundary condition the mean rate at which the particle reaches the boundary at $x = \delta$ starting at $x = 0$ is nothing but the steady state diffusion current $j_0 = -D\partial p/\partial x$.

The steady-state diffusion equation states that

$$\frac{\partial^2 p}{\partial x^2} = 0 \ , \tag{16.71}$$

which means that the probability is a linear function of position, i.e., $p(x) = Ax + B$. To compute the coefficients A and B we make use of two conditions: first we have the normalization condition,

$$\int_0^\delta p(x) d\, x = B\delta + A\frac{\delta^2}{2} = 1 \tag{16.72}$$

while the second condition ensures that the probability vanishes at $x = \delta$,

$$p(\delta) = A\delta + B = 0 \ ; \tag{16.73}$$

this is the condition that the particle will vanish when it reaches this boundary. From these two equations we find $A = -2/\delta^2$ and $B = 2/\delta$. The current is therefore

$$j_0 = -DA = \frac{2D}{\delta^2} \tag{16.74}$$

while the first passage time is the inverse of this quantity, $\tau_1 = \delta^2/2D$. The filament polymerization rate is then finally

$$v = \frac{\delta}{\tau_1} = \frac{2D}{\delta} \tag{16.75}$$

.

Now we can repeat the calculation in the presence of a force acting on the diffusing particle (in the case of the polymerization ratchet this would be the load). In this case the current also has a contribution from the drift produced by the applied force,

$$j_0 = -D\frac{\partial p}{\partial x} - \frac{F}{\gamma}p \tag{16.76}$$

where γ is the friction coefficient that relates the force to the velocity. The negative sign in front of the drift term is due to the fact that the force is taken to point in the negative x direction. The friction coefficient is related to the diffusion constant by the Einstein relation, $\gamma D = k_B T$. All of these ideas for treating driven diffusion were developed in sections 13.2.4 (pg. 695) and 13.2.5 (pg. 696).

In steady state the current is constant and we can solve the differential equation for $p(x)$ in terms of the unknown current j_0. The solution is the sum of the general solution of the homogeneous equation and a particular solution to the inhomogeneous equation:

$$p(x) = \underbrace{Ae^{-\frac{Fx}{k_B T}}}_{\text{homogeneous}} \underbrace{-j_0\frac{\gamma}{F}}_{\text{inhomogeneous}} \tag{16.77}$$

Since once again, $p(\delta) = 0$ and $\int_0^\delta p(x) = 1$ we get two equations for the two unknown constants, A and j_0, namely,

$$\begin{aligned} Ae^{-\frac{F\delta}{k_B T}} - j_0\frac{\gamma}{F} &= 0 \\ -A\frac{k_B T}{F}\left(e^{-\frac{F\delta}{k_B T}} - 1\right) - j_0\frac{\gamma}{F}\delta &= 1. \end{aligned}$$

These two equations yield a steady-state current of the form

$$j_0 = \frac{1}{\frac{k_B T\gamma}{F^2}\left(e^{\frac{F\delta}{k_B T}} - 1\right) - \frac{\gamma\delta}{F}} \tag{16.78}$$

which like in the no-force case leads to an expression for the polymerization rate

$$v = \delta j_0 = \frac{D}{\delta}\frac{(F\delta/k_B T)^2}{e^{F\delta/k_B T} - 1 - F\delta/k_B T}\ . \tag{16.79}$$

It is comforting to find that in the limit $F\delta \ll k_B T$ this expression reduces to the one obtained in the zero force limit. This makes intuitive sense since in this

case the thermal energy is so large that the diffusing "particle" does not "know" about the potential.

In the other limiting case, when $F\delta \gg k_BT$, the formula for the polymerization rate reduces to $v = F^2D\delta/(k_BT)^2 \exp(-F\delta/k_BT)$. This corresponds to a first passage time for the "particle" that is of the form, $\tau_1 = \delta/v = (k_BT/F)^2/D \exp(F\delta/k_BT)$. The prefactor is the time to diffuse a distance k_BT/F, while the exponential Arrhenius factor accounts for the probability that the particle finds itself with energy $F\delta$ while in thermal equilibrium at temperature T.

16.3.2 Force Generation by Growth

Polymerization Forces Can Be Measured Directly

Several techniques have been developed enabling direct measurement of forces generated by polymerizing filaments. The first direct measurement of force generated by polymerization of a single microtubule used the elastic beam properties of the microtubule itself as a transduction device to measure force. We have already discussed this experiment in fig. 10.33 (pg. 543), but there focused on calculation of the force needed to bend a microtubule. In actuality, the purpose of this experiment was not to measure the bending force, which was known through other means, but rather to measure the polymerization force generated at the interface between the growing microtubule and the wall and using the bending only as a readout. This classic experiment demonstrated that an individual microtubule can generate several piconewtons of actual pushing force while growing in this constrained geometry, as shown in fig. 16.47. This magnitude is similar to the force generated by a single kinesin or dynein motor as discussed earlier in this chapter.

Some complications arise from using the growing microtubule itself as the device to measure force generation. In particular, if the stiffness of the microtubule changes as it grows, a proposition for which there is experimental support, this may lead to an incorrect deduction of the force. It is therefore useful to have an independent way of measuring the polymerization force. This has been achieved using an optical trap as shown in fig. 16.48. As we have seen, optical traps are well suited for measuring forces in the piconewton range, with step sizes of several nanometers. These optical-trap based measurements are in excellent agreement with the measurements based on microtubule bending. This demonstrates that growth-dependent changes in microtubule flexibility are insufficient to significantly alter the interpretation of these measurements.

In vitro it is possible to measure forces generated by single motors, whether translational or polymerization motors. However, in cells it is rare for any kind of motor to operate in isolation. Most biological force generation involves arrays of cooperating force generating elements. Optical traps are not strong enough to measure the forces provided by a network of actin filaments. For this kind of measurement, the cantilever-based microscopies described in chap. 10 permit the investigation of much larger forces. As we showed in chap. 10, the stiffness

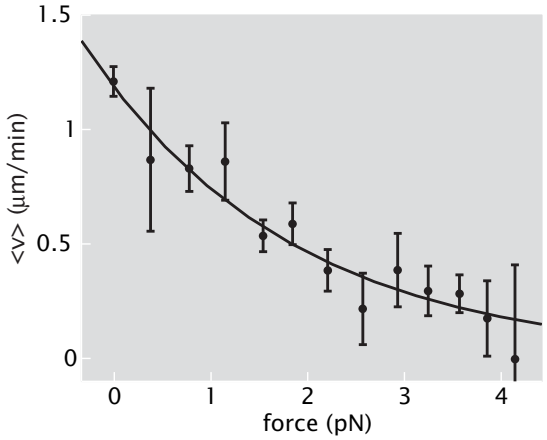

Figure 16.47: Average polymerization velocity for growing microtubules pushing up against a rigid barrier, as a function of applied force. In this experiment, the force was applied by the elastic bending of the growing microtubule itself. As for other molecular motors, the speed of the polymerization motor decreases as the force increases. (Adapted from M. Dogterom and B. Yurke, Science, 278:856, 1997.)

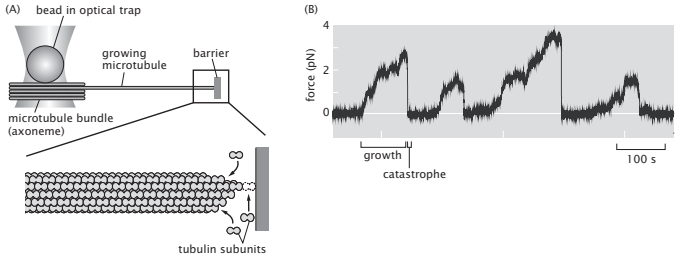

Figure 16.48: Optical trap measurement of the force of microtubule polymerization. (A) A bundle of microtubules is attached to a bead which is then held in an optical trap. The end of the trapped bundle is brought into close proximity of a rigid, nanofabricated wall. Addition of soluble tubulin dimers permits growth at the interface between the bundle and the wall, pushing the bead backward in the optical trap. (B) An individual trajectory measured for a single experiment reveals phases of microtubule growth followed by force-induced catastrophe. (Adapted from J. W. Kerssemakers *et al.*, Nature, 442:709, 2006.)

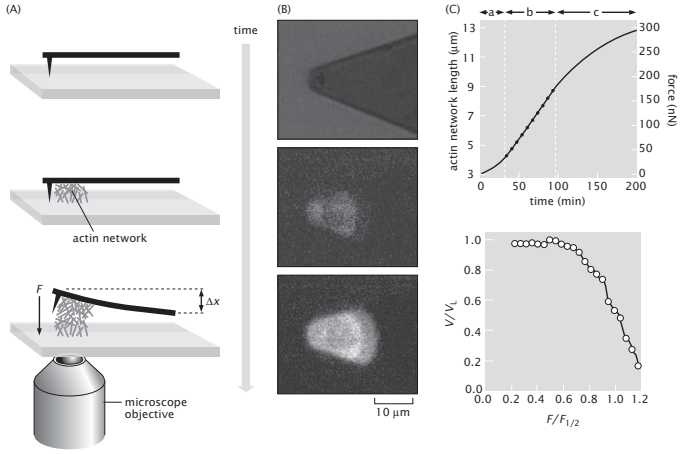

Figure 16.49: AFM measurement of polymerization forces. (A) Schematic of the experiment. A cantilever coated with a protein that promotes actin nucleation is brought close to a glass surface. When a solution is added containing actin monomers and crosslinking proteins, network growth is initiated on the cantilever. Continued network growth deflects the cantilever upwards. (B) Images of the cantilever photographed through the glass slide showing the accumulation of fluorescently labeled actin as the experiment progresses. (C) The top graph shows the total length of the actin network as a function of time. As the gel grows, the cantilever is deflected, and the amount of applied force increases. The bottom graph on the right shows the same data presented as a force-velocity curve for this experiment. The flat plateau on the left part of the graph indicates that network growth velocity remains constant even as force increases. (Adapted from S. H. Parekh *et al.*, Nat. Cell Biol., 7:1219, 2005.)

of a cantilever is a simple function of its thickness so the force range can be tuned. Fig. 16.49 shows a cantilever-based experiment where growth of an actin network was triggered to occur on the cantilever surface held in close proximity to a glass surface. Growth of the network deflecting the cantilever can be used to measure both force and growth velocity. This experiment demonstrated that arrays of actin filaments do not act together to generate force in a simple additive manner. Surprisingly, network growth occurs at a nearly constant rate over a large range of forces in contrast to all the individual molecular motors discussed so far which exhibit a monotonically decreasing force-velocity curve.

Polymerization Forces Are Used to Center Cellular Structures

The fact that cytoskeletal filament growth can produce pushing forces can be used by a cell to do much more than simply move. In particular, this phenomenon is exploited by cells to set up a universal coordinate system whereby they are able to locate their organelles at precise geographical locations in the

enormous cellular volume. Specifically, if microtubules within a cell are labeled fluorescently, it can be seen that they typically emanate in a star-like array from a single point known as the centrosome. The centrosome is a tiny object, less than 0.5 μm across, that nonetheless can position itself near the middle of a cell with typical sizes of tens of microns. How does the centrosome find the cell center? One possible mechanism can be demonstrated by a clever experiment illustrated in fig. 16.50 that involves isolating a centrosome and dropping it into a nanofabricated hole with dimensions comparable to those of a cell. The centrosome on its own diffuses around aimlessly. However, if tubulin is added so that microtubules can grow from the centrosome, the centrosome quickly (within minutes) zooms in to the geometric center of the hole, regardless of the hole shape. If the centrosome is grabbed with a laser trap and displaced from its central location, it will gently but insistently return to the center. The mechanism relies on the pushing forces at the tips of all of the microtubules when they run into the walls. Only when the centrosome is at the geometrical center of the enclosure do all of the forces cancel out. In living cells of the fission yeast *Schizosaccharomyces pombe*, this mechanism has been directly observed centering the nucleus halfway down this rod-shaped cell by virtue of microtubules pushing against the two opposite ends.

16.3.3 The Translocation Ratchet

Another fascinating kind of motor action introduced at the beginning of this chapter is associated with translocation. We argued that because of the division of cells into different compartments, there are a host of molecular machines whose job is to take polymers from one side of a membrane to the other (mechanisms like this might also be relevant for macromolecular assemblies like the proteasome). A schematic of the translocation process is shown in fig. 16.51. The polymer of interest is moving from left to right in the presence of a resistive force. By virtue of the action of binding proteins, the diffusive motion is ratcheted. The goal of this subsection is to examine the relation between the force and the velocity.

Protein Binding Can Speed Up Translocation Through a Ratcheting Mechanism

A rough quantitative feel for the speed up due to the presence of binding proteins and their associated ratchet action can be obtained by comparing the diffusion time in the absence and presence of the binding proteins. If we consider a polymer of length $L = nd$, then the time scale for diffusion motion over the entire length is

$$t_{\text{diffusion}} \approx \frac{n^2 d^2}{D}, \tag{16.80}$$

where d is the mean spacing between binding sites. The diffusive motion of a biopolymer traversing such a membrane will be sped up as a result of the binding of molecules to the polymer at a progression of sites once they have

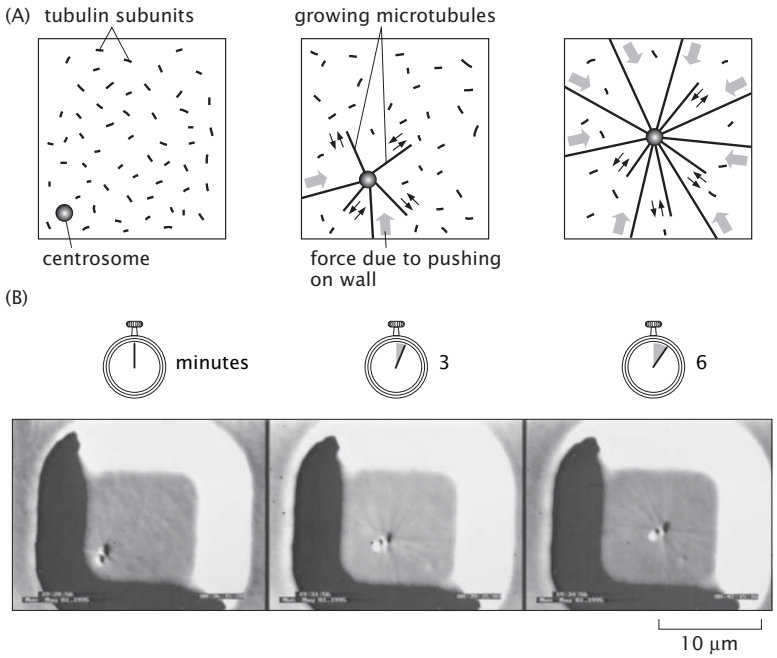

Figure 16.50: Self-centered centrosomes. (A) Diagrams showing time sequence of a self-centering experiment. Initially, a centrosome is added to a microfabricated square well along with soluble, tubulin subunits. As the centrosome nucleates growth of microtubules, individual microtubules grow and shrink in a process of dynamic instability. When a microtubule tip contacts the wall of the chamber, it can continue to grow resulting in a pushing force on the centrosome. Eventually, as microtubules grow longer and push against the wall in all directions, the centrosome finds a stable position of the geometrical center of the well. (B) Frames from a video sequence using differential interference contrast (DIC) microscopy show this process over a period of several minutes. (Adapted from T. E. Holy *et al.*, Proc. Nat. Acad. Sci., 94:6228, 1997.)

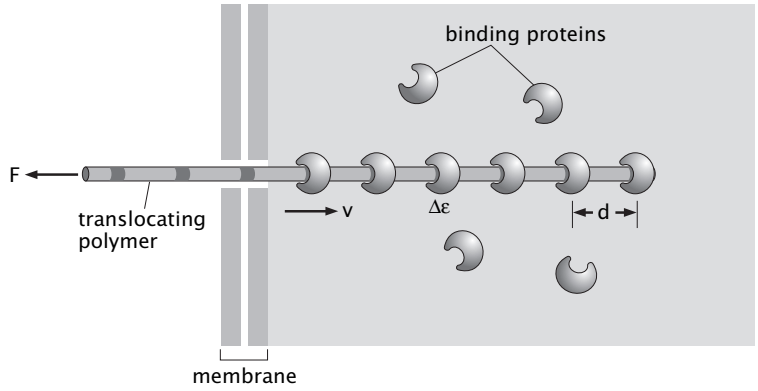

Figure 16.51: Translocation ratchet. Motion of a polymer across a membrane is ratcheted by the presence of binding proteins which prevent the back motion of the polymer.

crossed the membrane. In this case, the translocation time takes the form

$$t_{\text{translocate}} \approx n\frac{d^2}{D}. \tag{16.81}$$

This expression can be argued for simply by noting that d^2/D is the time for a single binding site to diffuse over a distance d. Assuming that this exposes the binding site to a binding protein, which then binds and prevents any backward motion of the polymer past this position, the total time for translocation is the time for all n binding sites to complete this process. That is, the speed up results from the fact that it is faster to make n diffusive trajectories of overall length d than it is to make a single diffusive trajectory to diffuse an overall distance nd.

In the case of a bacteriophage injecting its DNA into a bacterial cell the binding of RNA polymerases can serve to produce a ratchet effect (at the same time, of course, the RNA polymerase also performs the critical service of beginning to express the genes of the bacteriophage). For DNA with a characteristic length of 10 μm, typical of a genome of a bacterial virus, and with polymerase binding sites located roughly one per micron, the speed up due to polymerase binding will be $n = L/d = 10$. This will in fact be an upper bound given the fact that all binding is reversible and once in a while an RNA polymerase will detach from the DNA spoiling the ratcheting action. Because RNA polymerase is also a translational motor, it can probably also contribute to injection of the DNA genome by active energy-dependent movement. As we have previously discussed in chap. 10, the differential pressure between the bacteriophage capsid and the host cell cytoplasm can also contribute to the injection of DNA. However, other biological systems including the import of newly translated proteins into to the lumen of the endoplasmic reticulum and the delivery of cytoplasmically-

expressed proteins into the various compartments of the mitochondria appear to use mechanisms that can be schematized as translocation ratchets even though the relevant binding proteins are not themselves translational motors and there is no significant pressure differential.

To make these estimates more precise, we model the polymer as a rod diffusing through an opening (channel) in the membrane, the translocation pore. The polymer contains binding sites for proteins that cannot pass through the translocation pore, which are a distance d apart. We make a further simplifying assumption that the proteins are only present on one side of the membrane in the cellular compartment that the polymer in question is translocating *to*. We also assume that the binding of proteins is irreversible; the more realistic model would take into account the on and off rates for protein binding. The translocation process then proceeds in the following manner: The translocating polymer, buffeted by the solution, undergoes random diffusion through the translocation pore. By pure chance a protein binding site will find itself on the side where the binding proteins are present. If a protein then binds, the polymer will be prevented from diffusing back and it will have translocated by distance d. We can use this basic picture to calculate the average flux of protein binding sites through the translocation pore.

To address the question of translocation velocity we focus on the protein binding site which has *last* emerged from the pore. To describe the stochastic motion of this binding site we introduce the quantity $p(x,t)dx$, which is the probability of finding the last binding site to have crossed the pore at position $(x, x+dx)$ at time t. The translocation problem formulated in this way now maps to the Smoluchowski equation for the variable $p(x,t)$, the probability density. Namely, the flux of protein binding sites is given by

$$J_x = \underbrace{-\frac{Df}{k_BT}p}_{\text{Drift}} \underbrace{-D\frac{\partial p}{\partial x}}_{\text{Diffusion}} \tag{16.82}$$

where we have included a drift term to account for the possible presence of a force acting on the polymer during translocation; for $f > 0$ this is a force that opposes translocation. In the example of DNA translocation during viral infection a negative force is supplied during translocation by the host cells RNA polymerases, which help the translocation process along, speeding up the cells demise.

The Translocation Time Can Be Estimated By Solving a Driven Diffusion Equation

The differential equation that prescribes the evolution of the binding site probability is once again the Smoluchowski equation,

$$\frac{\partial p}{\partial t} + \frac{\partial J_x}{\partial x} = 0, \tag{16.83}$$

which in this case is the statement of the conservation of the number of binding sites, and is, upon substituting eqn. 16.82, the diffusion equation for $p(x,t)$.

"Well this is strange", a careful reader might complain, "we've arrived at the diffusion equation once again, so where is all the information about proteins, their binding sites, etc.". The answer is that this is what the boundary conditions are for! The boundary condition appropriate to our problem is

$$p(d,t) = 0 \tag{16.84}$$

which states that the probability of the protein binding site being at position $x = d$ is identically zero. This follows from the fact that we are following the motion of the last binding site to have emerged from the pore. As soon as this site finds itself at position d a new binding site emerges from the pore and binds a protein, and is now the new "last" site to emerge. The old "last" site effectively disappears at this point.

To calculate the steady-state current ($J = \text{const}$) we solve $J_x = J$ with the boundary condition eqn. 16.84, essentially exactly as we did in the previous section for the polymerization motor. The solution to the homogeneous part of the resulting differential equation is

$$p_{\text{hom}}(x) = Ce^{-\frac{fx}{k_BT}} \tag{16.85}$$

while

$$p_{\text{part}}(x) = -J\frac{k_BT}{Df} \tag{16.86}$$

is a particular solution; the sum of the two is the general solution with C a constant that can be determined from the boundary condition. After a bit of algebra we arrive at

$$p(x) = J\frac{k_BT}{Df}\left(e^{\frac{f(d-x)}{k_bT}-1}\right) \tag{16.87}$$

which gives us the probability of finding the last protein binding site to have crossed the pore a distance x away from the pore, *in the steady state* (thus the lack of any time dependence).

At this point we should remind ourselves of the original goal we set out to accomplish. We are really interested in the translocation velocity for the polymer in the steady state v_{tr}, which is simply related to the current J: $v_{\text{tr}} = Jd$. In order to calculate J we make use of the fact that the probability of finding the last protein site anywhere on the interval $(0, d)$ is one, i.e.,

$$\int_0^d p(x)dx = J\frac{d^2}{D}\left(\frac{k_BT}{fd}\right)\left[e^{\frac{fd}{k_BT}} - \frac{fd}{k_BT} - 1\right] = 1. \tag{16.88}$$

Finally, solving the above equation for the steady state current leads to a formula for the translocation velocity as a function of the force acting on the polymer

$$v_{\text{tr}} = \frac{D}{d}\frac{w^2}{e^w - w - 1} \tag{16.89}$$

where $w = \frac{fd}{k_BT}$ is the dimensionless force. Note that in the small load force limit we arrive at a simple expression, $v_{\text{tr}} = 2D/d$ which follows from a simple

argument: the time for the protein binding site to diffuse over a distance d unassisted by an applied force is $d^2/2D$; once this occurs a new protein is bound and the polymer has translocated by distance d. Therefore, the translocation velocity is given by $d/(d^2/2D) = 2D/d$, same as above.

In a more realistic model of translocation, the irreversibility of the protein binding should be relaxed. Instead one has on and off rates for the binding of these proteins. This will enter the model described above, again, through the boundary condition for $p(x)$ in the equation for the steady state current. The main qualitative difference that this imparts on the predicted translocation velocity dependence on the force is the emergence of a finite stall force at which $v_{\rm tr}$ goes to zero. In the model worked out above, eqn. 16.89 leads to an infinite stall force, which is an unphysical feature.

16.4 Summary and Conclusions

Directed forces in biological systems are powered by molecular motors devoted to the conversion of chemical energy into mechanical energy. Although their detailed mechanisms and biological functions are impressively diverse, we have shown in this chapter that many aspects of motor function can be fruitfully considered by breaking motor activity down into a series of small, discrete steps. Transitions between steps can be considered using either discrete or continuous formalisms that acknowledge differences in energy for different internal motor states and also the influence of diffusive and stochastic events. Many mechanical properties of motors including speed, force or torque, power and variability can be thus considered in a unifying theoretical framework.

16.5 Problems

1. Randomness in the one-state model An alternative definition for the randomness to that given in the chapter is

$$r = \lim_{t\to\infty} \frac{\langle x(t)^2\rangle - \langle x(t)\rangle^2}{a\langle x(t)\rangle}. \tag{16.90}$$

(a) Using the definition of randomness given above and the probability distribution for the one-state motor in the continuum model of eqn. 16.16, work out an explicit expression for the randomness.
(b) Eqn. 16.24 provides an expression for the randomness in terms of the force-dependent rate constants. Using the model in which all of the force dependence is in the forward rate, obtain an expression for the randomness and make a plot of its force dependence.

2. Stepping of myosin V Single molecule experiments have been performed on myosin V where a fluorescent marker was placed at different locations on the

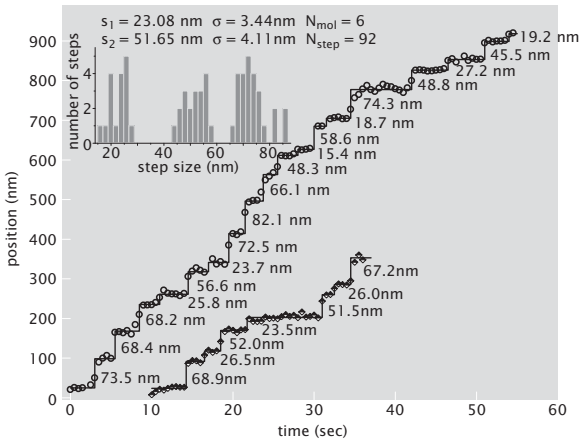

Figure 16.52: Single molecule measurements of steps taken by mysoin V along actin filaments. The histogram in the inset is of all the measured step sizes, which are measured with 1.5 nm precision. (Adapted from A. Yildiz *et al.*, Science, 300:2061, 2003.)

light-chain domain (one of the two "legs of the motor) and individual steps were recorded. It was found that the average step size is about 37 nm; see fig. 16.52.
(a) If the dye is placed on the light-chain domain a distance x from the mid-point between the two heads of the motor (the "feet that bind to the actin filament) and along the direction of motion of myosin V, what step sizes do you expect to observe. What value of x explains the data shown in fig. 16.52?
(b) Assume that the stepping rate is k. This is the probability per unit time that the motor will make a step. Calculate the expected waiting time distribution between two steps observed in experiments, if the fluorescent marker is placed at position x found in part (a). What is the expected distribution, assuming a hand-over-hand stepping mechanism, if the marker is placed very close to one of the heads (ie., $x \approx 37$ nm)? Use your calculated distributions to rationalize and fit the data from the Yildiz *et al.* paper provided on the book web site. Does your analysis support the hand-over-hand mechanism? What value of k do you obtain?

3. Kinesin as an ATP hydrolyzing enzyme

As described in the chapter, careful measurements have been performed which examine the dependence of motor velocity on ATP concentration. Under certain conditions the hydrolysis reaction performed by a molecular motor can be described using the Michaelis-Menten model introduced in section 15.2.7 (pg. 783). In the particular case of kinesin its stepping is strongly coupled to its ATPase activity, which translates into relatively constant step sizes. Finally, its high processivity allows for a clear definition of a speed since it gets to do many steps before falling off from the microtubule.

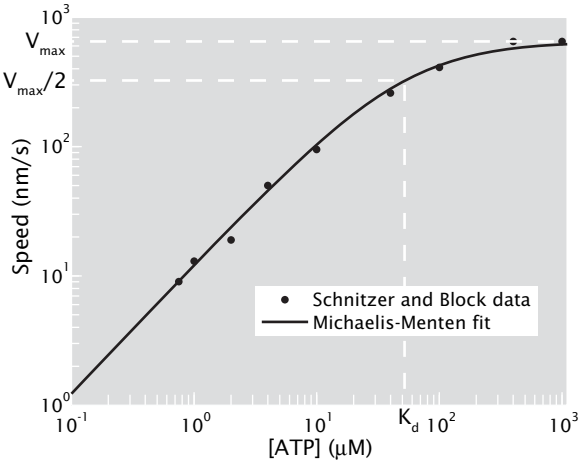

Figure 16.53: Michaelis-Menten kinetics. Speed of a kinesin motor as a function of ATP concentration and fit of the data to a Michaelis-Menten model. (Adapted from M. J. Schnitzer and S. M. Block, Nature, 388:386, 1997.)

Relate the reaction speed (the rate of ATP hydrolysis) to the maximum stepping speed of kinesin and determine its dependence on ATP concentration. Work out what change in substrate concentration is needed to increase the reaction rate from $0.1v_{max}$ to $0.9v_{max}$. Finally, fit your model to the data by Schnitzer and Block shown in fig. 16.53.
Relevant data for this problem is provided on the book web site.

4. Kinetics of two-state motors In the chapter, in order to obtain the velocity of a two-state motor, we made use of a trick to circumvent solving the master equation directly. Here we take upon this task and in the process also derive an expression for the randomness.
(a) Consider a trial solution of the system of equations for $p_0(n,t)$ and $p_1(n,t)$, given by eqns. 16.33 and 16.34, which is of the form

$$\begin{pmatrix} p_0(n,t) \\ p_1(n,t) \end{pmatrix} = e^{\imath(Kn-\omega t)} \begin{pmatrix} A \\ B \end{pmatrix}. \tag{16.91}$$

Find a relation between K and w that guarantees the existence of a solution of this form. This is the so-called dispersion relation.
(b) By substituting the trial solution $\exp(\imath(Kx-\omega t))$ into the differential equation for diffusion with drift (eqn. 13.54), show that the dispersion relation in this case is

$$\omega = vK - \imath DK^2.$$

(c) We now demonstrate that in the limit $K \ll 1$ the dispersion relation for the two-state motor is the same as that for diffusion with drift. To do this

Taylor expand $\omega(K)$ in K and solve the equation for ω obtained in part (a) order by order in K, which amounts to computing the coefficients in the Taylor expansion. Compare your result to the dispersion relation for dispersion with drift and read off the diffusion coefficient for the motor and its speed. Check that the formula for the speed matches the one obtained in the chapter.

5. Myosin and Muscles: Some Estimates In the chapter we described (very briefly) the organization of muscles. In this problem, we will examine this in more detail.
a) Give a "multiscale" description of muscles. That is, describe the various levels in the structural hierarchy of muscles starting with the entire muscle itself (at the largest scales) and ending with the individual myosin molecules (at the smallest scales). Make sure you discuss each structural feature in some detail, making sure to describe the relevant length scales.
b) Make an estimate of the cross-sectional area of a muscle and work your way through to the maximum force available during contraction of the muscle by figuring out the force available per molecule (again, think about a cross section). You will probably have to refer to some of the single molecule work on myosin to really carry out a correct estimate (see Howard, pg. 267, for example). In particular, once you have your estimate of the number of myosins per cross section and the force available per myosin, you will be able to make a preliminary estimate (although not all myosins are attached at all times and you may want to consider that also).

6. Polymerization ratchet estimates.

In the chapter we analyzed the polymerization ratchet in the two limiting cases of diffusion limited and reaction limited polymerization. By comparing the time for a load, a polystyrene sphere 1 μm in diameter, to diffuse a distance given by the actin monomer size, and the average time for an actin monomer to be added to the growing end of the filament, find the condition for the free actin monomer concentration that is necessary for the polymerization in the presence of the load to be reaction limited. Compare this concentration with the critical concentration for actin filament growth.

16.6 Further Reading

S. Vogel, **Prime Mover - A Natural History of Muscle**, W. W. Norton and Company, New York: New York, 2001. Like all of Vogel's books, this one makes for fascinating reading and is pertinent to part of the story developed in this chapter.

J. Howard, **Mechanics of Motor Proteins and the Cytoskeleton**, Sinauer Associates, Inc., Sunderland: Massachusetts, 2001. Howard's book is the first source that we go to when trying to learn more about motors.

T. Duke, "Modelling Motor Proteins" in **Physics of Bio-molecules and Cells**, edited by H. Flyvbjerg, F. Jülicher, P. Ormos and F. David, EDP Sciences, Springer-Verlag, Les Ulis: France, 2002. An instructive discussion of motor proteins.

P. Nelson, **Biological Physics: Energy, Information, Life**, W. H. Freeman and Company, New York: New York, 2004. Very interesting discussion of motor proteins.

M. E. Fisher and A. B. Kolomeisky, "The force exerted by a molecular motor", Proc. Nat. Acad. Sci., **96**, 6597 (1999).

M. E. Fisher and A. B. Kolomeisky, "Simple mechanochemistry describes the dynamics of kinesin molecules", Proc. Nat. Acad. Sci., **98**, 7748 (2001). This interesting paper examines how simple models like those described in the chapter can respond to single-molecule data on motor dynamics.

N. Thomas, Y. Imafuku and K. Tawada, " Molecular motors: thermodynamics and the random walk", Proc. Roy. Soc. London **B268**, 2113 (2001).

L. Mahadevan and P. Matsudaira, "Motility powered by supramolecular springs and ratchets", Science, **288**, 95 (2000). This interesting review summarizes several exotic kinds of force generation that we do not address.

F. Jülicher, A. Ajdari and J. Prost, "Modeling molecular motors", Rev. Mod. Phys. **69**, 1269 (1997). A comprehensive review with many useful and general insights into motor function.

S. M. Simon, C. S. Peskin and G. F. Oster, "What drives the translocation of proteins?" Proc. Nat. Acad. Sci.. **89**, 3770 (1992). An important and thought provoking paper on the translocation ratchet.

J. A. Theriot, "The Polymerization Motor", Traffic, **1**, 19 (2000). This review summarizes the theoretical basis for force generation by filament assembly.

C. S. Peskin, G. M. Odell and G. F. Oster, "Cellular motions and thermal fluctuations: the Brownian ratchet", Biophys J., **65**, 316 (1993). This beautiful paper describes the physics of motors like those described in the tail end of our chapter.

R. Zandi, D. Reguera, J. Rudnick and W. M. Gelbart, "What drives the translocation of stiff chains?" Proc. Nat. Acad. Sci., **100**, 8649 (2003). More recent insights into the nature of translocation ratchets.

16.7 References

S. M. Block, L. S. Goldstein and B. J. Schnapp, "Bead movement by single kinesin molecules studied with optical tweezers" Nature, **348**, 348 (1990).

C. Bustamante, D. Keller and G. Oster, "The physics of molecular motors", Acc. Chem. Res., **34**, 412 (2001).

C. Bustamante, Y. R. Chemla, N. R. Forde, and D. Ishaky, "Mechanical processes in biochemistry" Ann. Rev. Biochem., **73**, 705 (2004).

M. R. Diehl, K. Zhang, H. J. Lee and D. A. Tirrell, "Engineering cooperativity in biomotor-protein assemblies", Science, **311**, 1468 (2006).

M. Dogterom and B. Yurke, "Measurement of the Force-Velocity Relation for Growing Microtubules", Science, **278**, 856 (1997).

J. C. Gebhardt, A. E. Clemen, J. Jaud and M. Rief, "Myosin-V is a mechanical ratchet", Proc. Nat. Acad. Sci., **103**, 8680 (2006).

N. Hirokawa, "Kinesin and Dynein Superfamily Proteins and the Mechanism of Organelle Transport", Science, **279**, 519 (1998).

T. E. Holy, M. Dogterom, B. Yurke and S. Leibler, "Assembly and positioning of microtubule asters in microfabricated chambers", Proc. Nat. Acad. Sci., **94**, 6228 (1997).

J.W. Kerssemakers, E. L. Munteaunu, L. Laan, T. L. Noetzel, M. E. Janson and M. Dogterom, "Assembly dynamics of microtubules at molecular resolution", Nature, **442**, 709 (2006).

A. B. Kolomeisky and M. E. Fisher, "A simple kinetic model describes the processivity of myosin-v", Biophys J., **84**, 1642 (2003).

J. C. Liao, J. A. Spudich, D. Parker and S. L. Delp, "Extending the absorbing boundary method to fit dwell-time distributions of molecular motors with complex kinetic pathways", Proc. Nat. Acad. Sci., **104**, 3171 (2007).

A. D. Mehta, R. S. Rock, J. A. Spudich, M. S. Mooseker and R. E. Cheney, "Myosin-V is a processive actin-based motor", Nature, **400**, 590 (1999).

H. Noji, R.Yasuda, M. Yoshida and K. Kinoshita Jr., "Direct observation of the rotation of F1-ATPase", Nature, **386**, 299 (1997).

S. H. Parekh, O. Chaudhuri, J. A. Theriot and D. A. Fletcher, "Loading history determines the velocity of actin-network growth", Nat. Cell Biol., **7**, 1219

(2005).

T. J. Purcell, C. Morris, J. A. Spudich and H. L. Sweeney, "Role of the lever arm in the processive stepping of myosin V", Proc Nat. Acad. Sci., **99**, 14159 (2002).

T. J. Purcell, H. L. Sweeney and J. A. Spudich, "A force-dependent state controls the coordination of processive myosin V", Proc. Nat. Acad. Sci., **102**, 13873 (2005).

D. I. Rodionov and G. G. Borisy, "Self-centring activity of cytoplasm", Nature, **386**, 170 (1997).

M. J. Schnitzer, K. Visscher and S. M. Block, " Force production by single kinesin motors", Nat. Cell Biol., **2**, 718 (2000).

M. J. Schnitzer and S. M. Block, "Kinesin hydrolyses one ATP per 8-nm step", Nature, **388**, 386 (1997).

L. Turner, W. S. Ryo and H. C. Berg, "Real-time imaging of fluorescent flagellar filaments" J. Bacteriol., **182**, 2793 (2000).

R. D. Vale, "The molecular motor toolbox for intracellular transport", Cell, **112**, 467 (2003).

K. Visscher, M. J. Schnitzer and S. M. Block, "Single kinesin molecules studied with a molecular force clamp", Nature, **400**, 184 (1999).

R. Yasuda, H. Noji, K. Kinosita Jr. and M. Yoshida, "F1-ATPase is a highly efficient molecular motor that rotates with discrete 120 degree steps", Cell, **93**, 1117 (1998).

A. Yildiz, J. N. Forkey, S. A. McKinney, T. Ha, Y. E. Goldman and P. R. Selvin, "Myosin V Walks Hand-Over-Hand: Single Fluorophore Imaging with 1.5-nm Localization", Science **300**, 2061 (2003).